Bulletin of Volcanology (2026) 88:57
https://doi.org/10.1007/s00445-026-01974-w

RESEARCH

Forecasting future instability hazards at Anak Krakatau volcano, Indonesia, using archival reconstructions of edifice evolution

Kerys Meredew[1] · Sebastian F. L. Watt[1] · Mike Cassidy[1] · Achmad Fakhrus Shomim[2] · Muhammad Edo Nurshal[3,4] · Mirzam Abdurrachman[4] · Muhammad Hanif[2,5] · Wilfridus F. S. Banggur[2] · Dini Nurfiani[2] · Samantha Engwell[6] · Victoria C. Smith[7] · Chiara M. Petrone[8] · Carl T. E. Stevenson[1] · Devy Kamil Syahbana[9]

Received: 7 October 2025 / Accepted: 4 April 2026

Abstract

Volcanic lateral collapses represent major hazards through associated eruptive activity, landslide inundation and, in island or coastal settings, the generation of tsunamis. Forecasting the timing, precursory indicators, and magnitude of lateral collapses still remains a significant gap in volcanic risk management, a challenge exemplified by the 2018 lateral collapse of Anak Krakatau, Indonesia. The volcano's southwestern flank collapsed without recognised warning, resulting in a devastating tsunami which inundated > 300 km of regional shorelines. Since then, the edifice has rapidly regrown, prompting a necessary assessment of its future stability. Here we analyse Anak Krakatau's uniquely detailed archival growth records, in combination with satellite and drone datasets, to reconstruct historical edifice development from 1919 to 2023, using this to then project and contextualise its future growth trajectories and assess potential instability conditions. Our time series of 3D models reveals that post-collapse regrowth has mimicked historical development trends, but on a considerably accelerated timescale. If future growth follows the long-term pre-collapse (1960–2018) average, then a subaerial edifice morphology equivalent to 2018, but with larger overall dimensions, would be met by around the year 2100. If future development maintains the much higher 2019–2023 growth trends, then a morphology comparable to 2018 could instead be reached by the 2030s. We consider the continuation of such high growth rates unlikely, but this highlights the importance of monitoring edifice growth and flank instability signals over the coming decades, following the methodology provided here. Additionally, the submarine SW flank now has a considerably reduced gradient relative to 2018, which is likely to promote stability further into the future. To comprehensively assess future stability, the role of alteration, hydrothermal activity and the structure of the submarine flank should also be evaluated.

Second Language Abstract (Indonesian)

Runtuhan lateral gunung api merupakan bahaya besar yang dapat memicu aktivitas erupsi, tanah longsor, serta—khususnya pada lingkungan pulau atau pesisir—pembentukan tsunami. Namun, kemampuan untuk memprediksi waktu kejadian, indikator pendahulu, dan besarnya runtuhan masih menjadi tantangan utama dalam manajemen risiko vulkanik. Hal ini ditunjukkan oleh peristiwa runtuhan Gunung Anak Krakatau pada tahun 2018 di Indonesia. Lereng barat daya gunung tersebut runtuh tanpa adanya peringatan dini yang teridentifikasi, sehingga memicu tsunami yang menghancurkan dan menggenangi lebih dari 300 km garis pantai di wilayah sekitarnya. Setelah kejadian tersebut, tubuh gunung api telah mengalami pertumbuhan kembali dengan cepat, sehingga diperlukan evaluasi terhadap stabilitasnya di masa depan. Dalam penelitian ini, kami menganalisis catatan arsip pertumbuhan Anak Krakatau yang sangat rinci, dikombinasikan dengan data satelit dan drone, untuk merekonstruksi perkembangan morfologi tubuh gunung api selama periode 1919–2023. Rekonstruksi kemudian digunakan untuk memproyeksikan pertumbuhan di masa depan serta menilai potensi ketidakstabilannya. Rekonstruksi model 3D secara temporal yang dihasilkan menunjukkan pertumbuhan kembali pasca-runtuhan 2018 mengikuti pola perkembangan historis, namun terjadi pada skala waktu yang lebih cepat. Apabila pertumbuhan mengikuti rata-rata pertumbuhan sebelum runtuhan

Editorial responsibility: M. Edmonds

Extended author information available on the last page of the article

Published online: 30 April 2026

(1960–2018), morfologi tubuh gunung api yang setara dengan kondisi tahun 2018 diperkirakan akan tercapai sekitar tahun 2100, meskipun dengan dimensi keseluruhan yang lebih besar. Sebaliknya, apabila tren pertumbuhan yang jauh lebih tinggi pada periode 2019–2023 berlanjut, morfologi yang sebanding dapat tercapai pada sekitar tahun 2030. Meskipun laju pertumbuhan yang sangat tinggi ini berkemungkinan kecil, hasil ini menegaskan pentingnya pemantauan pertumbuhan tubuh gunung api serta sinyal ketidakstabilan lereng dalam beberapa dekade mendatang, sebagaimana pendekatan metodologis yang disajikan dalam penelitian ini. Selain itu, lereng barat daya bawah laut saat ini memiliki kemiringan yang lebih landai, sehingga dapat meningkatkan stabilitas di masa depan. Untuk memperoleh penilaian stabilitas yang lebih komprehensif, proses alterasi batuan, aktivitas hidrotermal, serta struktur lereng bawah laut juga perlu dipertimbangkan.

Keywords Volcanic edifice growth · Lateral collapse · Tsunami · Historical volcanology · Eruption forecasting · Volcanic landslides

Introduction

Large-scale gravitational collapses are a fundamental process affecting volcanoes across all volcano-tectonic settings. The development of oversteepened slopes, internal structural heterogeneities, and hydrothermal alteration ultimately produces structures prone to instability (Siebert 2002; van Wyk de Vries and Davies, 2015; Roverato et al. 2021). Such collapses often involve > 10% of the total edifice volume (Watt 2019) and can result in a series of cascading and complex hazards, including mass movements, landslide inundation, explosive volcanism and, in island settings, large-magnitude tsunamis. They therefore pose significant risks to exposed populations (Watt et al. 2019; Keating and McGuire 2000; Manzella et al. 2024).

Growing evidence suggests that cycles of edifice growth and destruction, through variable loading of the underlying magma system, exert an important control on eruption rates and magma storage on a range of timescales (Pinel et al. 2010; Watt 2019; Cutler et al. 2022). Lateral collapses interrupt edifice growth trajectories and may therefore mark important transitions in the eruption rate, volcano behaviour and the structural development of volcanoes. However, our capacity to investigate these relationships in detail is limited; most volcanoes are constructed over thousand-year timescales, meaning that pre-historical phases of activity are generally buried or eroded, and can at best only be reconstructed at low resolution from the stratigraphies of dispersed eruption products. Few lateral collapses have been observed globally, and understanding their precursors, timing, consequences and driving factors remains a major challenge.

In contrast, Anak Krakatau (Indonesia) is a young volcano which has grown rapidly since its first emergence above sea level in 1928. Its collapse, just 90 years later, provides a unique opportunity to examine a complete volcanic development cycle, and thereby advance our knowledge of the drivers of volcanic lateral collapse. Through integrating archival reports, photos and topographic maps with remote sensing techniques, we have developed a time series of 3D reconstructions (and accompanying eruption records) of Anak Krakatau from 1919 to 2023. Using this historical context, we then project future growth scenarios, considering both volumetric and morphological equivalents to the 2018 collapse. This not only provides an important route to evaluating the future stability of Anak Krakatau as the edifice regrows, but also provides an analogue for understanding edifice development and stability globally. Ongoing instability monitoring is key to developing improved risk management strategies in the densely populated region surrounding Anak Krakatau, where the partially submerged setting and frequent eruptions present a particularly challenging set of linked landslide, eruption and tsunami hazards.

Geological and historical background

Krakatau is a partially submerged caldera volcano located within the Sunda Strait, between Sumatra and Java, Indonesia. Its catastrophic 1883 caldera-forming eruption was responsible for an estimated 36,000 fatalities, resulting primarily from a tsunami generated during the eruption's final explosive stages (Verbeek 1885; Sigurdsson et al. 1991; Self 1992). The initial phases of this eruption involved a series of NNW-aligned vents (Fig. 1; Madden-Nadeau et al. 2021); this same alignment broadly coincided with the NE margin of the 1883 caldera, suggesting caldera faulting exploited the main volcano feeder system (Self 1992; Deplus et al. 1995). The next documented volcanism at Krakatau occurred in 1927, originating from a series of submarine vents along the same NNW alignment (Umbgrove 1928; Stehn 1929a). This resurgence in activity marked a distinct change in eruptive composition, shifting from the rhyodacites erupted in 1883 to basaltic andesite magma (Camus et al. 1987; Gardner et al. 2013).

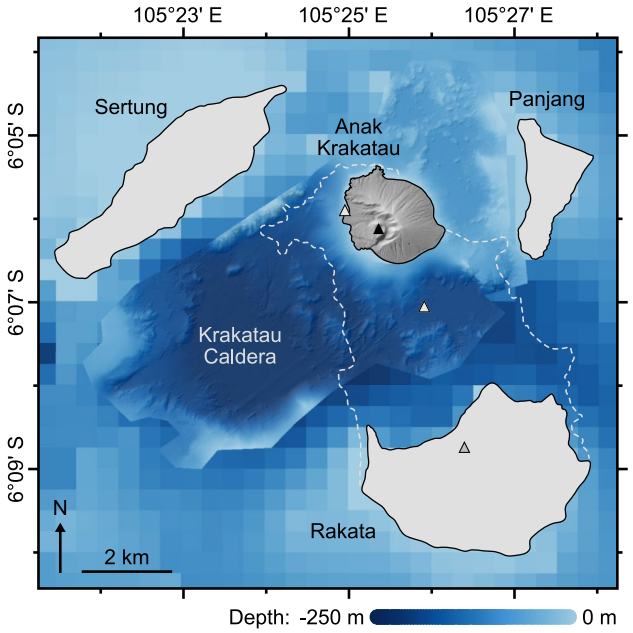

Fig. 1 Location of Anak Krakatau relative to the submerged 1883 Krakatau Caldera, with the current active vent indicated by the black triangle. Krakatau's approximate pre-1883 subaerial extent is marked by the grey dashed line (Verbeek, 1885; Judd 1888), with the three grey triangles indicating the former NNW vent alignment. Rakata is the southernmost remnant of the pre-1883 Krakatau edifice; Sertung and Panjang are the remnants of an earlier, pre-historic edifice (Verbeek, 1885; Judd 1888). Bathymetry within the caldera is from 2019 (Hunt et al. 2021), with GEBCO (2024) in the background. Topographic data for Anak Krakatau was acquired in 2023

Repeated eruptions eventually generated the new permanent island of Anak Krakatau by 1930 (Stehn 1930; Neumann van Padang 1933, 1983). Reconstructed bathymetry from 1919 (Escher 1919; Stehn 1929a) shows that this island developed at the edge of the NE margin of the 1883 caldera, on a shallow marine shelf ~50 m below sea level (mbsl) (Fig. 1). To the SW of this point, the caldera scarp sloped steeply (~24°) towards the centre of the caldera basin (~279 mbsl); to the NE, the seafloor gradually declined (~8°) to ~100 mbsl. As material accumulated around the active vent, it rapidly deposited on the low-angle shelf NE of the vent, but on the SW side of the vent, material was readily transported downslope into the caldera basin, resulting in significantly slower accumulation. This ultimately led to an inherent asymmetry of the island (and a recognised instability of the SW side; Giachetti et al. 2012), which has influenced the volcano's morphology and growth throughout its history.

Anak Krakatau has been frequently active since 1927 (Fig. 2; Table 2), with each eruptive phase progressively constructing the island. The edifice reached its maximum dimensions in December 2018, when a large-scale landslide removed all subaerial material from the SW sector, including the summit region. The collapse orientation was broadly parallel to the caldera scarp, following a NW–SE line across the centre of the edifice and creating an unusually wide opening angle (approaching 180°) for a volcanic lateral collapse. Within this paper, we use this structural alignment to divide the edifice into two sectors (the SW and NE), cutting through the current vent position. This transect also correlates with the top of the underlying 1883 caldera scarp, located using the 1919 bathymetry (Escher 1919; Stehn 1929a), and follows the same lineament as the 1940 s shoreline erosion of Anak Krakatau. Dividing the edifice in two enables us to investigate the relative growth rates and surface loading on either side of this structural boundary, evaluating the potential for future instability of the SW flank. This is particularly important as intense volcanic activity following the 2018 collapse has resulted in the rapid regrowth of the island.

Methods

Using 29 historic topographic surveys, alongside satellite- and drone-derived digital elevation models (DEMs), we have developed a time series of 3D-reconstructions spanning Anak Krakatau's subaerial growth from 1929 to 2023 (Table 1), enabling calculation of island volume (km^3) and surface area (km^2). This entire process was completed in QGIS (version 3.28.2 Firenze; QGIS.org 2026), whilst utilising accompanying archival morphological descriptions, images (Online Resource 1 and 2) and eruption accounts for further context. Submarine growth has additionally been reconstructed, although at a lower resolution due to limited bathymetric data, to estimate total volcanic output.

Historical reconstructions

Scanned topographic and bathymetric maps were loaded into QGIS (using CRS WGS 84/UTM Zone 48S) via the Raster Georeferencer tool, using the map's grid coordinates. Where coordinates were not available, maps were georeferenced based on the location of the NE crater rim (a persistent feature throughout much of the volcano's history), whilst ensuring scaling remained consistent.

Once georeferenced, the topography was digitised by manually plotting elevation points (in metres) along mapped contour lines to generate a GeoPackage point file (.gpkg). A DEM was generated from each .gpkg file using the SAGA Natural Neighbour interpolation module (Conrad et al. 2015). This method is designed for grid interpolation from irregularly distributed points, using elevation as the input attribute, Sibson as the interpolation method and a Cell size of 1. Subaerial island volume and surface area were then calculated for all DEMs using the Raster Surface Volume tool (relative to a base level of 0 m).

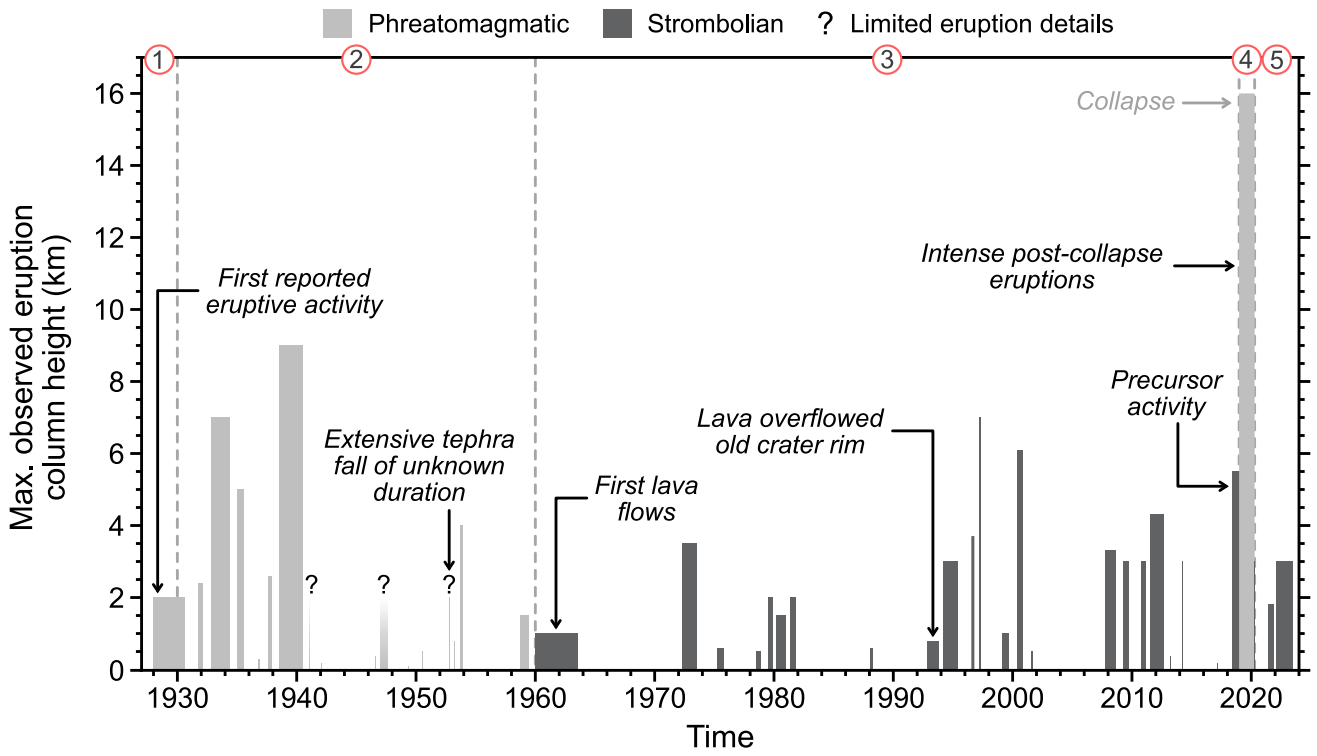

Fig. 2 Overview of Anak Krakatau's eruptive record, summarising the key changes in reported style, duration, and maximum eruption column height (km) for each observed eruptive phase, spanning from December 1927 through to June 2023. Data is collated from numerous sources outlined in the historical activity catalogue provided in Online Resource 1. Red circled numbers at the top of the figure refer to development stages discussed throughout

Estimating reconstruction uncertainty

Several areas of potential uncertainty are introduced during the topographic reconstruction and DEM generation process, via the interpolation method, the digitised resolution, data point positioning and the original map quality. Exploration of these uncertainties is described in detail in the extended methods (Online Resource 3) and shows that the major source of uncertainty is the (unquantifiable) accuracy of the original maps, rather than the processing uncertainty introduced by subsequent analytical decisions. However, as a large number of maps (29) can be independently analysed, and demonstrate self-consistent growth patterns, we conclude that these maps are sufficiently accurate to not introduce any significant systematic error into the calculated growth rates.

The processing uncertainty was evaluated for both the interpolation method and the digitisation. The influence of the DEM interpolation method on volumetric calculations is minimal. Across five tested high-resolution topographic maps (spanning varied island morphologies, from April 1929, August 1935, October 1941, August 1947 and October 1953), the calculated volumes differed by an average of +0.038% (Linear) and −0.016% (Non-Sibsonian) relative to Sibson interpolation.

Each DEM will also be influenced by the number of digitised contours within the corresponding.gpkg file. Unfortunately, the quality of mapped contours varies considerably across the original maps. In some cases, printing and reproduction errors have resulted in image distortions, and in others the tight spacing of lines results in specific contours becoming indistinguishable. To evaluate this influence, the five test maps were digitised using all contours (defined as 100% digitised resolution), with contours then successively removed to reduce the resolutions. Calculated volumes decreased by an average of 0.18% at 75% digitised resolution, and then by 0.51% and 2.16% at 50% and 25% resolution, respectively. Of our 29 reconstructed maps, 15 could be digitised using all contours. The remainder could all be plotted to at least 75% digitised resolution (any below this threshold were not used in our dataset). A similar protocol for assessing uncertainty has been applied to maps with contour spacings greater than 5 m (i.e. lower quality maps). For example, the January 2019 topographic map has contours at 10 m intervals, resulting in a digitised resolution of 50% relative to a 5 m contour map, and we therefore assume a volume uncertainty of ± 0.51%.

In this way, we have estimated processing uncertainties for all maps based on their contour resolution and the

Table 1 Topographic, bathymetric, satellite- and drone-derived data sources used to reconstruct Anak Krakatau's growth history from 1919 to 2023. See Online Resource 3 for an extended version, including resolution and uncertainty estimates

Date	Data type	Source
1919	Digitised bathymetric survey	Escher 1919; Stehn 1929a
1929 April 1930 July and Aug 1933 March and Oct 1935 Feb, Aug and Dec 1936 June, Aug and Dec 1937 Feb and Dec 1938 June, Aug and Oct 1939 June and Aug 1940 Dec	Digitised topographic surveys	Bulletin of the Netherland Indies Volcanological Survey*, multiple surveys spanning 1929–1941
1941 Oct 1947 Aug	Digitised topographic surveys	De Neve 1951
1950 Sept 1952 Oct 1953 Oct 1960 Jan	Digitised topographic surveys	Decker and Hadikusumo 1961
1963 March	Digitised topographic survey	Zen and Hadikusumo 1964
1985 Aug	Digitised topographic survey	Thornton and Rosengren 1988
1990	Digitised topographic survey	Partomihardjo et al. 1992
1990 Sept	Digitised bathymetric survey	Deplus et al. 1995
2012	Satellite	Badan Informasi Geospasial (BIG) 2012
2018 Dec (pre-collapse)	Adapted satellite	Gouhier and Paris 2019; Grilli et al. 2021
2018 Dec (post-collapse)	Resected pre-collapse DEM	*This paper*
2019 Jan	Digitised topographic map (original data acquired via drone survey)	Gouhier and Paris 2019
2019 Aug	Bathymetric survey	Hunt et al. 2021
2019 Aug 2021 June 2023 June	Drone surveys	*This paper (surveys by BRIN and ITB, Indonesia)*

*In some texts the former Netherland Indies Volcanological Survey is also referred to as either the Netherlands East Indian or the Netherlands India Volcanological Survey

interpolation method. These uncertainties do not propagate significantly and are therefore given as a summed percentage for each DEM (Online Resource 3).

Erosion correction

Since Anak Krakatau's first subaerial emergence (1928), the island's pyroclastic deposits have been subject to continual erosion, as evidenced by the fluctuation in shoreline morphology and deep gullying. Tuffs, deposited from phreatomagmatic eruptions and prone to rapid coastal erosion, formed the entirety of the island until 1960 and continue to make up much of the shoreline and surficial deposits. To estimate erosional volume loss, a constant erosion rate of -1.95×10^{-7} km^3/year per metre of shoreline formed by tuff has been applied to each period of subaerial volumetric growth. This rate is derived from the absolute volume reduction between October 1941 and August 1947 (-8.70×10^{-4} km^3/year), normalised to the shoreline distance (4466 m). This interval represents the longest available period (~6 years) spanned by high-resolution topographic surveys and without significant eruptive activity. Additionally, 1941 did not follow a major eruptive phase, which could result in an anomalous and short-lived post-eruption erosional pulse. We therefore consider the 1941–1947 period as representative of the long-term background tuff erosion rate. This estimated rate was compared with three other shorter periods of volume reduction, which all implied broadly similar erosion rates.

Incorporating bathymetry

To calculate total erupted volume between 1919 and 2019, we combined post-collapse bathymetry from Hunt et al. (2021) with a drone-derived DEM of the island, both surveyed in August 2019. Gaps in merging these datasets were resolved by manually interpolating contours at 1–10 m intervals. Digitised bathymetry from 1919 (derived from point soundings; Escher 1919; Stehn 1929a), representing the seafloor prior to growth of Anak Krakatau, was then subtracted

to calculate the total volume of material emplaced between these two points. This material is assumed to be entirely derived from Anak Krakatau volcanism. On the steep caldera walls, resolution of the 1919 bathymetry is relatively poor, resulting in a few isolated discrepancies where the 1919 interpolated depth is shallower than that measured in 2019. As these areas only occur on the western caldera margin, which in general shows a close match to the 2019 bathymetry but with minor sediment accumulation since 1919, we consider these areas to all be artefacts within the 1919 bathymetry rather than reflecting true areas of caldera deepening. We have therefore clipped these artefacts to avoid negative growth values. The difference between the 1919 and 2019 bathymetry shows thick sediment accumulation on the caldera floor, likely to have accumulated both via direct fallout and post-eruption erosion. Because Anak Krakatau's eruptions are generally low in intensity, the majority of its eruptive products are likely to be contained within this surrounding marine basin, and we consider our estimate to therefore be a reasonable estimate of total output from the volcano. It does not, however, account for material deposited on the surrounding islands of Panjang and Sertung (Fig. 1) or at greater distances offshore. Our observations of deposit thicknesses on Panjang and Sertung show the total Anak Krakatau fall deposit thickness to reach a maximum of 1.5 m (totalling an estimated 0.013 km^3 deposited across the two islands), declining to tens of centimetres away from the main axes of ash plume dispersal (Urlaub et al. 2023). From this, we infer that material beyond the local marine basin represents < 1% of the total output of Anak Krakatau and is not likely to affect our 1919–2019 estimate significantly.

After 1919, bathymetric data for the caldera region is extremely limited, with only one additional survey from 1990 available (Deplus et al. 1995). Detailed analysis of the volcano's submarine growth is therefore not possible. As such, we use island development (i.e. only the subaerial portion) to provide a high-resolution proxy for examining the output rates from Anak Krakatau as a whole, which can then be scaled against the total volcanic output, evaluated from the 1919–2019 bathymetric and topographic change.

Calculating edifice density and mass

To estimate loading across the edifice, mass (kg) has been calculated using the subaerial volume (km^3) and estimates of rock density. The subaerial edifice can be broadly separated into two lithological types: tuff derived from Surtseyan phreatomagmatic activity, representing all activity at Anak Krakatau until 1960 (Decker and Hadikusumo 1961); and lava representing the lava flows and central pyroclastic cone constructed around the vent and over much of the western portion of the island from 1960 to 2018, alongside more minor fall deposits on the eastern flank. The shift in activity in 1960 directly results from the vent becoming subaerial and the crater lake becoming infilled. This removed seawater interaction and led to a switch from phreatomagmatic to purely magmatic eruption styles. The DEM produced for 1960 is taken as the discontinuity surface between the two lithological types, i.e. tuff for all pre-1960 materials, and lava (broadly capturing both lava flows and the pyroclastic cone) for all post-1960 materials. This surface aligns closely with the 2018 collapse scar, suggesting that edifice instability, at least in part, was influenced by this lithological boundary. Post-collapse, a further lithological transition occurred, repeating the pre-/post-1960 pattern, but over a significantly shorter timescale; very rapid island regrowth occurred via tuff deposition until December 2019, after which a subaerial pyroclastic cone and lava flows once again formed. For this second transition, the closest DEM we have is from August 2019, and so this is taken to represent the post-collapse lithological discontinuity. Figure 3 summarises this simplification of lithological types across the edifice.

Density of the two lithologies was calculated using the measured volume (via water displacement) and mass of hand-sized rock samples from Anak Krakatau. Only one consolidated tuff sample was available for Anak Krakatau, with a density of 1.69 g/cm^3. Published density values from Surtsey (Iceland) were used to assess the validity of this estimate; Surtsey is a young mafic volcanic island, which rapidly developed from the seafloor following a series of offshore eruptions between 1963 and 1967 (Thorarinsson 1967; Moore 1985). Tuff drilled from the subaerial portion of the edifice in 1979 and 2017 had a measured density of 1.39–1.66 g/cm^3 (Oddsson 1982; Jackson et al. 2019), suggesting that our tuff estimate is a realistic representation of Surtseyan-derived deposits. Anak Krakatau lava flow samples from 1995, 2012 and 2017 had densities of 2.28, 2.44 and 2.23 g/cm^3 (averaged to 2.315 g/cm^3). However, this density likely represents a maximum value for the lava lithology. This is because part of the emplaced mass during the 1960–2018 and 2019–2023 periods was scoriaceous, accumulating as a pyroclastic cone around the vent, and not as lava flows. Our DEM analyses indicate this cone represents approximately 25% of the volume erupted in the 2019–2023 post-collapse period; assessments of the pre-collapse edifice are more challenging due to the lower temporal resolution of topographic data. There are very few estimates of the bulk density of pyroclastic cones, and since the cone is likely formed by interbedded lavas and scoriaceous material, a precise estimate cannot be obtained. Nevertheless, a bulk density estimate of 1.39 g/cm^3 from the Omuroyama cone, Japan (Nagahara et al. 2022), enables us to estimate a lower bound on the average density of erupted material during subaerial Anak Krakatau activity. Using a 75:25 lava to cone ratio, and the two density values above, results in a value of 2.08 g/cm^3. We

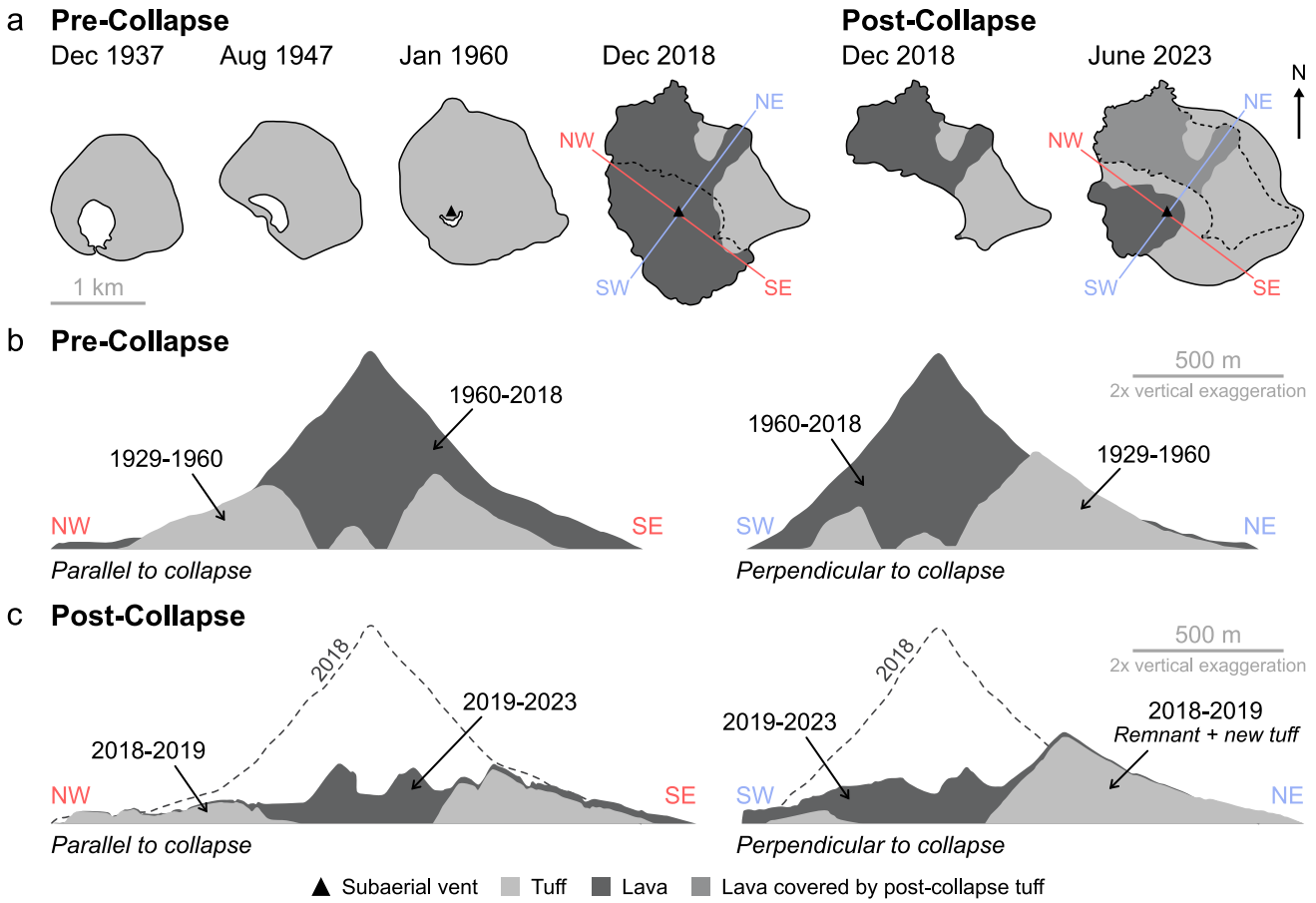

Fig. 3 Schematic evolution of Anak Krakatau's major subaerial morphological stages (**a**) and the inferred internal lithological boundaries (**b** and **c**) used for edifice mass calculations. **a** NW–SE transect (red) denotes the division of the edifice into two sectors (SW and NE) used in projecting future growth; SW–NE transect (blue) is perpendicular to this and follows the 2018 collapse direction. **b** Prior to the 2018 collapse, the tuff-lava boundary is marked by the 1960 transition to Strombolian eruptions and the emplacement of lava flows (derived from the January 1960 DEM). **c** After the 2018 collapse, this transition occurred with the re-initiation of lava flows in April 2020, estimated here from the August 2019 DEM

use our measured lava density (2.315 g/cm^3) in subsequent analysis, as it is our only direct estimate of erupted material from Anak Krakatau's subaerial eruptive phases, but we also draw on this lower bound (2.08 g/cm^3) to indicate the likely range of mass loading. For future projections of instability at Anak Krakatau, where our interest is in when the edifice will reach an equivalent form to the 2018 failure conditions, the absolute density is a minor uncertainty, given that the partitioning between different materials (lava, scoria) is likely to be similar between the 1960–2018 and the post-2019 periods.

Results

Anak Krakatau's pre-collapse eruptive and morphological history can be broadly divided into three stages (Table 2): the initiation of volcanism (1927–1930), a phreatomagmatic phase (1930–1960) and a fully subaerial phase characterised by Strombolian to Vulcanian activity (1960–2018). Post-collapse, eruptive activity can be split into two phases: intense post-collapse phreatomagmatic eruptions (2018–2019; stage 4), followed by the return to a subaerial vent and lava flows (2019 onwards; stage 5). Within each of these stages, activity is then further subdivided into a series of distinct eruptive periods, separated by periods of extended inactivity (with a minimum repose requirement of 2 weeks); the end of each eruptive period is defined as a cessation of observable magmatic activity at the surface. The duration of these periods is a minor uncertainty, as they rely on eruptive activity being both observed and subsequently recorded in historical archives, but these do not impact our calculated output rates. Complete historical and photographic catalogues detailing each known eruptive episode (with attributed collated sources) can be found in Online Resources 1 and 2. The growth history is summarised in Fig. 4.

Table 2 Summary of Anak Krakatau's eruptive stages, from the onset of volcanism in December 1927 through to June 2023. Full source details are provided in Online Resource 1. In this table and throughout the paper and online resources, all numerical dates are written in DD–MM–YYYY format

Stage		Dates	Dominant eruption style	Max. reported eruption column height (km)	No. of eruptive periods	Average eruptive period (days)	Average repose (days)
Pre-Collapse	1	29–12–1927 to 15–08–1930	Surtseyan	2	14	31	40
	2	15–08–1930 to 25–06–1959	Phreatomagmatic	9	42	32	223
	3	16–12–1959 to 22–12–2018	Strombolian	7	23	231	714
Post-Collapse	4	22–12–2018 to 30–12–2019	Intense phreatomagmatic	15	1	373	0
	5	30–12–2019 to 12–06–2023	Strombolian	3	3	256	245

Stage 1: initiation of volcanism (1927–1930)

The resurgence of volcanism within the Krakatau Caldera was reported by local fishermen on 29 December 1927, describing columns of "smoke" and glowing bombs visible by night (Umbgrove 1928; Stehn 1929a; Neumann van Padang 1933). Initiation may have predated this, with one earlier report potentially consistent with submarine eruptions in 1913 (Anon 1915), though this remains uncertain and no submarine volcanic structure is evident in bathymetry from Escher (1919). Eruptive activity in 1927 was characterised by intermittent cycles of violent Surtseyan ash explosions generating eruption columns of up to 2 km (Fig. 2; Table 2), followed by periods of water fountaining, gas-bubbling and steaming (Neumann van Padang 1951). Reports suggest this early volcanism originated from six submarine vents, aligned NNW–SSE across approximately 500–600 m (Umbgrove 1928; Stehn 1929a).

During this stage, Anak Krakatau's eastern crater wall partially emerged above sea level on three separate occasions, before its final establishment as an island on 11 August 1930 (Stehn 1930; Neumann van Padang 1933, 1983). Its first appearance in January 1928 lasted ~1 week, forming an elongated island, 3 m high and 175 m in length (Stehn 1929a). The second occurred in January 1929 for ~22 weeks (Fig. 5a and b), during which several height measurements were taken, alongside one topographic survey dated April 1929 (Fig. 5c). The reported height peaked at 38 m on 18 February 1929, having averaged ~1.8 m of vertical growth a day. This was followed by decline (due to erosion), with the island disappearing by 3 July 1929. The crater wall then reappeared above the water for the third time in June 1930, remaining subaerial for ~8 weeks. On 1 July 1930, the peak of the island was measured at 50 m (Fig. 5d), with reports of destruction during violent activity thereafter (Neumann van Padang 1933). The final emergence, and establishment of Anak Krakatau as the present-day volcanic island, occurred on 11 August 1930 and was surveyed shortly after on 15 August 1930 (Fig. 5f). At this stage, the island's reconstructed subaerial volume was 0.0024 km^3 and surface area 0.50 km^2. The active vent remained below sea level throughout (Fig. 4).

Stage 2: phreatomagmatic dominated activity (1930–1960)

During Stage 2 (1930–1960), volcanism remained episodic (Fig. 2; Table 2). Activity generally consisted of dark ash-rich plumes of varying magnitude, often as multiple sustained pulses occurring in quick succession (e.g. Stehn 1933, 1937, 1938; Van Bemmelen 1941; De Neve 1951). Explosivity reached its observed maximum on 18 June 1939, producing a 9 km eruption column (Stehn 1940). Structural development consisted of rapid but fluctuating growth, with episodes of prolonged quiescence and erosion. Development of an enclosed (but low lying) crater wall and crater lake, with recurring breaches, meant that explosivity continued to be driven by magma-seawater interaction (Neumann van Padang 1951; Hedervari 1986).

By 9 October 1941, the island's reconstructed subaerial volume totalled 0.053 km^3 (Fig. 4a), with a surface area of 1.60 km^2. Most of this erupted material accumulated on the relatively flat, shallow seafloor to the NE (in contrast with the deeper, steeper slopes of the 1883 caldera scarp to the SW), resulting in a highly asymmetric form. Relative inactivity during the 1940s resulted in a substantial retreat of the southwestern shoreline (Fig. 6d–f) and by 21 August 1947, an island volume and area loss of 9.6% and 16.1%, respectively. This reduction occurred entirely in the SW sector, opening the crater to the sea, with the NE sector continuing to grow. Records from this time are limited due to World War II and its aftermath (Hedervari 1986), possibly resulting in missing eruption details.

Short-lived, powerful eruptions during the 1950s re-enclosed the active vent, with this development documented by four topographic surveys (September 1950, October 1952, October 1953 and January 1960). Reports from June 1959 document the development of a small central cone (Fig. 7a and b), approximately 25 m high and 200 m across, partially displacing the crater lake (Decker 1961). By 1960,

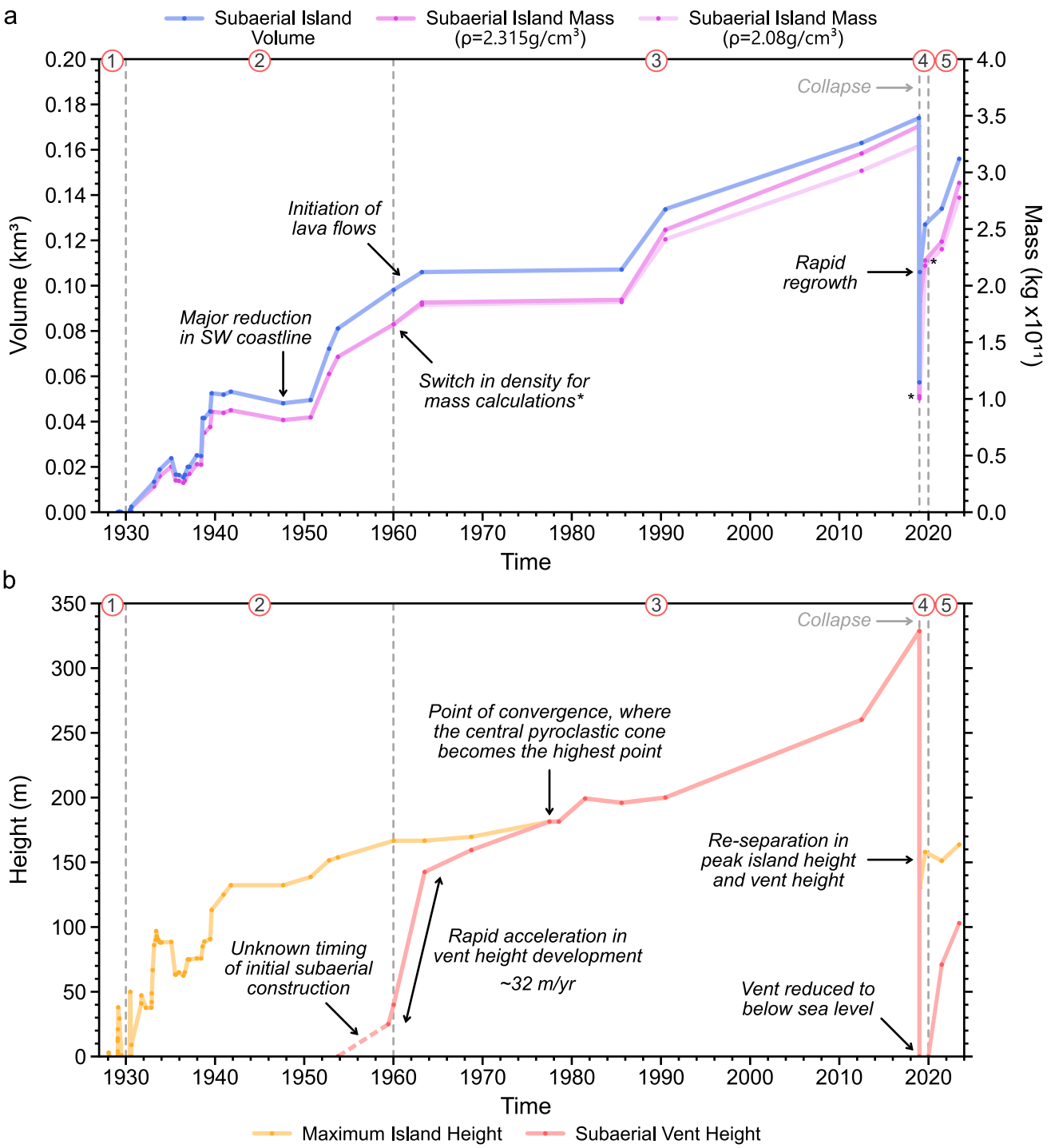

Fig. 4 Anak Krakatau's volumetric, mass and height development (1927–2023). **a** Subaerial island volume (km^3; blue) is calculated from 3D-reconstructions of historical maps, combined with satellite and drone derived datasets. Subaerial island mass ($kg \times 10^{11}$; purple) is calculated using volume reconstructions and density estimates (note mass is provided as an upper and lower bound using an estimated density range for the lava lithology, as per the discussion of densities within the methods). Changes in density are marked by an asterisk (*). The estimated volume uncertainty is too small to view at the scale of the graph. **b** Maximum reported island height (orange) and vent height measured from the central pyroclastic cone (pink), both in metres. Maximum island height is measured from the eastern crater rim throughout, until the central pyroclastic cone (vent) becomes the highest point ca. 1977. Maximum island height and vent height then become separated again following collapse. Red circled numbers refer to development stages discussed throughout

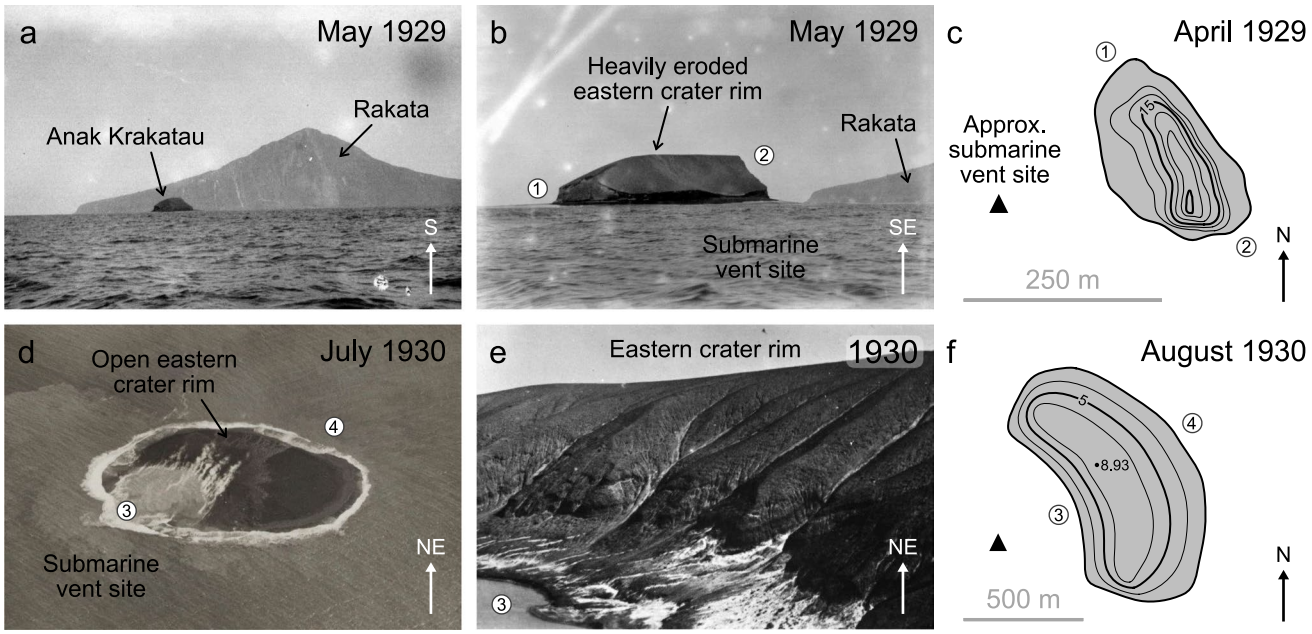

Fig. 5 Stage 1 (1927–1930): Subaerial development of Anak Krakatau during the initiation of volcanism. **a** and **b** May 1929; a portion of the heavily eroded eastern crater rim (~30 m height), with steep cliffs to the NW and SE (points 1 and 2). Rakata in the background is ~813 m high (van der Sleen 1929b, 1929a). **c** Reconstructed topography from April 1929 (based on Stehn 1929b), during the volcano's second subaerial emergence (first volume estimate within this study). The submarine vent site was ~150 m offshore (black triangle); contours are at 5-m intervals. **d** Aerial photograph of the third subaerial emergence in July 1930 (~50 m high). The eastern crater rim is open towards the west (point 3), and the active vent remains submerged (Unknown 1930). **e** Incised gullies on eastern crater wall in 1930/1933 (date uncertain; KNILM 1930; Neumann van Padang 1933). **f** Reconstructed topography from August 1930, with the island's peak at 8.93 m (based on Stehn 1930); contours are at 2.5-m intervals

the cone was fully cut off from seawater interaction (Fig. 7c and d) (Decker and Hadikusumo 1961; Hadikusumo 1961a). The reconstructed island volume totalled 0.098 km^3 by January 1960, with maximum island height reaching 167 m and the active vent at ~40 m (Fig. 4b).

When accounting for erosion, the reconstructed subaerial volumetric growth rate from August 1930 to January 1960 was 0.0043 km^3/year (non-erosion corrected: 0.0032 km^3/year). The NE sector of the edifice accounted for 77.6% of the total island volume and 75.7% of the surface area.

Stage 3: Strombolian dominated activity (1960–2018)

The 1960 s marked the transition to subaerial activity, although some reports suggest that phreatomagmatic eruptions still occurred infrequently, likely relating to the incursion of seawater through cracks and fissures (Decker and Hadikusumo 1961; Zen 1970). Activity generally consisted of dark ash-laden columns typically reaching 2–3 km, with lower intensity lava fountaining. Lava flows were first reported between 1960 and 1963 (Decker and Hadikusumo 1961), with further periodic flows through to 2018 (De Neve 1985; Abdurrachman et al. 2018). These lavas extended the western coastlines significantly; due to the pre-existing topography, they were confined to the SW sector, building out the island in a direction that had previously been dominated by coastal erosion. By 1993, material had infilled the pre-1960 crater and extended over the rim to the east (Global Volcanism Program 1993).

Historical data becomes more limited after 1960, with only three topographic surveys used herein (March 1963, August 1985 and 1990). The survey resolution also becomes significantly lower, with wider contour spacing of up to 25 m; additional surveys from 1972 and 1981 were rejected due to their very low resolution. Two satellite-derived DEMs dated 2012 (DEMNAS) and December 2018 (Gouhier and Paris 2019; Grilli et al. 2021) have been used alongside the topographic surveys. Topographic data from the Shuttle Radar Topography Mission (SRTM) in 2000 substantially overestimates the lower flank elevation and is therefore not included.

From 1960 through to 2018, subaerial island volume increased by 77.0%, reaching a calculated pre-collapse total of 0.174 km^3 in December 2018 (Fig. 4a). Growth rates were relatively stable throughout this period, associated principally with the emplacement of material at the centre of the island. Initially, vent height developed rapidly, increasing by 103 m between 1960 and 1963 (~32 m/year), then slowing to a longer-term average of ~3 m/year (Fig. 4b). The central vent formed the island's peak from ca. 1977 onwards,

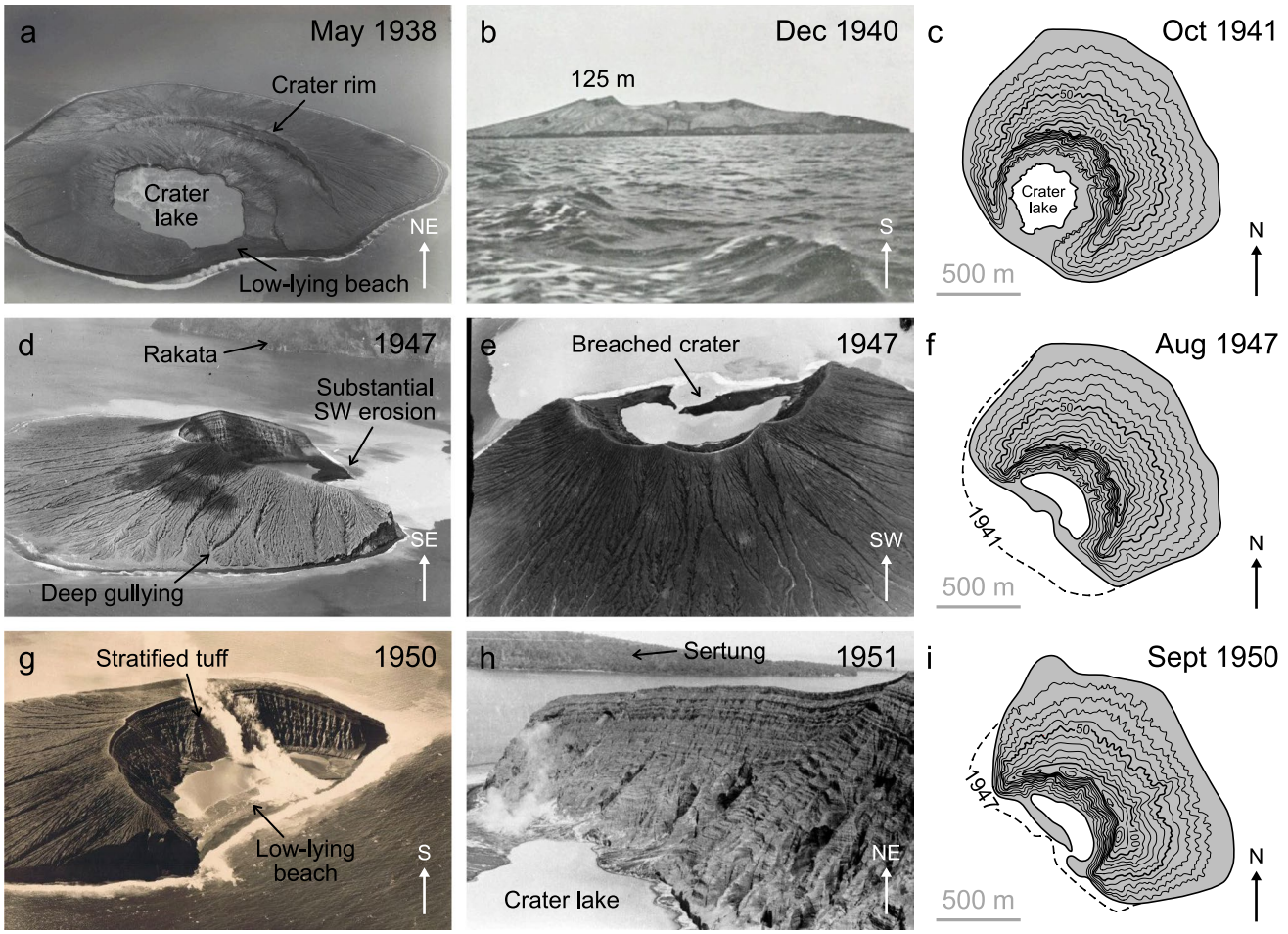

Fig. 6 Mid stage 2: Limited eruptive activity coupled with sustained erosion throughout the 1940s resulted in the retreat of Anak Krakatau's SW coastline, likely reaching its peak loss around 1947–49. **a** Aerial photograph from May 1938 (KNILM 1938). **b** December 1940 topographic profile, viewed from the north (height 125 m) (Van Bemmelen 1941). **c** Reconstructed topography from October 1941 (based on De Neve 1951); height 132 m, contours are at 10-m intervals. **d** Shoreline erosion and deep flank gullies in 1947 (Petruschevsky 1947). **e** Aerial photograph from 1947 (White 1947). **f** Reconstructed topography from August 1947 (based on De Neve 1951); contours are at 10-m intervals. **g** Aerial photograph from 1950 (Huiskamp 1950). **h** Crater interior in 1951, showing well stratified phreatomagmatic tuff and steep seaward cliffs (Unknown 1951). **i** Reconstructed topography from September 1950 (based on Decker and Hadikusumo 1961), showing the further retreat of the SW shore from 1947, but growth in height (139 m). Contours are at 10-m intervals

reaching a pre-collapse maximum of ~330 m. During this period, the surface area increased by 37.3% to 2.85 km^2, as lava deltas expanded the westerly coastlines (Fig. 3a) and the island grew in height.

The long-term erosion corrected volumetric growth rate from January 1960 to December 2018 (pre-collapse) was 0.0018 km^3/year (non-erosion corrected, 0.0013 km^3/year). The NE sector of the edifice accounted for 60.3% of total subaerial volume and 65.1% of total surface area.

The 2018 lateral collapse and post-collapse regrowth

Anak Krakatau's southwestern flank collapsed on 22 December 2018 between 13:55 and 13:57 (UTC), following a period of heightened but not atypical eruptive activity. The full event sequence prior to and immediately following the collapse is described in detail elsewhere (e.g. Grilli et al. 2019; Walter et al. 2019; Perttu et al. 2020; Priyanto et al. 2021; Cutler et al. 2022).

We estimate an initial post-collapse reconstruction by resecting the December 2018 DEM based on the coastline geometry observed within the Sentinel-1 IW-DV [dB] orthorectified satellite image captured on 22 December 2018 at 22:33:44 (UTC), approximately 8 hours after collapse. This was supported by interpretation of aerial photographs and video footage from 23 December 2018, which precisely capture where the failure plane cut the pre-collapse lava deltas to the northwest and southeast. The collapse removed all subaerial material from the SW sector, including the summit

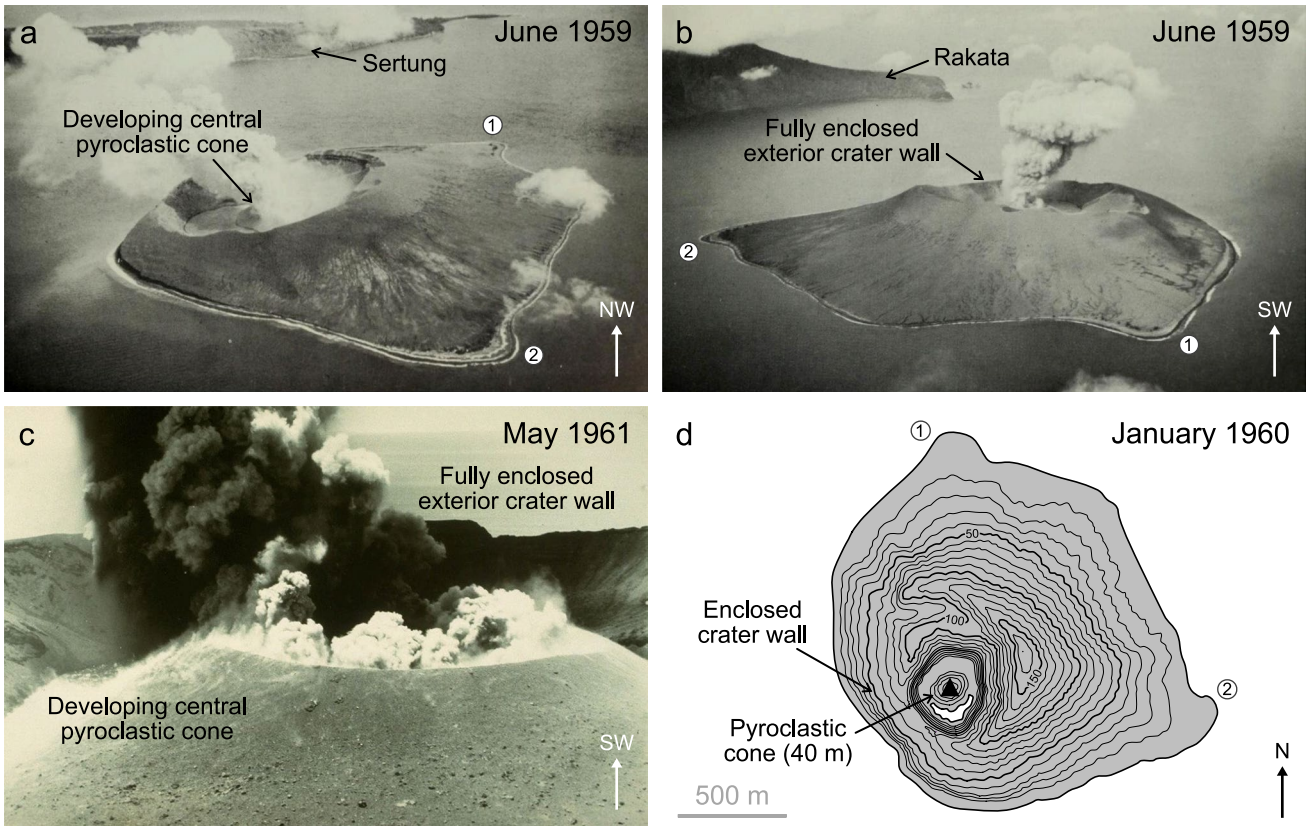

Fig. 7 End stage 2 to early stage 3: **a** and **b** Aerial photographs of Anak Krakatau in June 1959 showing the fully enclosed exterior crater wall and a small central pyroclastic cone (~25 m high) (Furneaux 1964). **c** Activity at the newly constructed pyroclastic cone (height unknown) in May 1961 (Hadikusumo 1961b). **d** Reconstructed topography from January 1960 (based on Decker and Hadikusumo 1961), with island height of 167 m and cone height of 40 m; contours are at 10 m intervals, and the black triangle marks the subaerial vent

region, reducing the island's surface area by 46.7% and subaerial volume by 67.0%—a total subaerial volume loss of 0.116 km^3 (Fig. 4a). Our reconstruction gives a post-collapse island height of 152 m, corresponding to the approximate position of the 1950s eastern crater rim.

Four drone-derived topographic surveys have been used to constrain post-collapse regrowth, from 10 January 2019 (digitised from Gouhier and Paris 2019), 15 August 2019, 26 June 2021 and 12 June 2023 (surveyed by BRIN and ITB, Indonesia).

Stage 4: intense phreatomagmatic regrowth (2018–2019)

Eruptive activity drastically shifted immediately after the lateral collapse; the active conduit was cut below sea level, with the incursion of seawater driving violent phreatomagmatic explosions (Grilli et al. 2019; Walter et al. 2019; Cutler et al. 2022). New pyroclastic material rapidly accumulated across the edifice, infilling the collapse scar within a few days, extending the NE coastline and producing a distinct rounding of the shoreline. By 10 January 2019, just 19 days after the collapse, Anak Krakatau's subaerial volume totalled 0.106 km^3 (Fig. 4a), an increase of 84.6% and equivalent to 10 years of growth during the previous phreatomagmatic phase (e.g. 1950–1960).

Growth via tuff deposition produced a low-profile island with smooth coastal form, similar to the pre-1960 volcano, albeit on a larger scale. During these 19 days, island surface area increased by 97.2%, whilst island height reduced by a further 18 m (relative to our immediate post-collapse DEM). This reduction may have been a consequence of minor degradation and erosion of the collapse scar during the violent post-collapse Surtseyan activity, but may also reflect imprecision in the 2018 DEM. PlanetScope satellite imagery from 7 January 2019 shows the re-establishment of a circular crater lake approximately ~250 m in diameter, which expanded to ~450 m by 12 January 2019. The crater lake's level remained constant (at sea level) despite intense evaporation, suggesting a subsurface connection to the surrounding sea (Novellino et al. 2020). There is no strong evidence for a shift in the post-collapse vent location relative to the pre-collapse period, as has been suggested

previously (Williams et al. 2019). After January 2019, island development slowed with the diminishing eruptive activity; volume increased by 19.8% in the 7 months to August 2019. Deposition increased the island height to 158 m, whilst coastal erosion resulted in a surface area loss of 0.7%.

From the collapse in December 2018 through to August 2019, the average erosion corrected growth rate was 0.108 km^3/year (non-erosion corrected, 0.107 km^3/year); this rate is strongly skewed by the extremely high late-December/early-January growth. Most of this post-collapse subaerial growth (79.2%) was on the NE sector, which by August 2019 accounted for 88.6% of the total edifice volume (78.0% of the area). There must have additionally been extensive deposition within the submarine scar region (to the SW), which is not accounted for by the DEMs.

Stage 5: return to Strombolian activity (2019–2023)

The exact timing of the subaerial re-emergence of Anak Krakatau's vent is uncertain; partially obscured satellite imagery from 30 December 2019 shows a vapour plume and substantial deposition of fresh tephra which appears to have infilled much of the crater lake. This is confirmed by photographs from 6 January 2020 (Fig. 8a–d), which show the subaerial cone and only a remnant of the crater lake NW of the vent. Activity from this point was Strombolian in style, producing dense grey-black ash-rich plumes extending up to 3 km (Global Volcanism Program 2023). The first clear sighting of post-collapse lava flows was on 17 April 2020 (Fig. 8e), infilling the remnant crater lake and extending the coastline to the west. A second lava flow occurred in April 2022, first visible

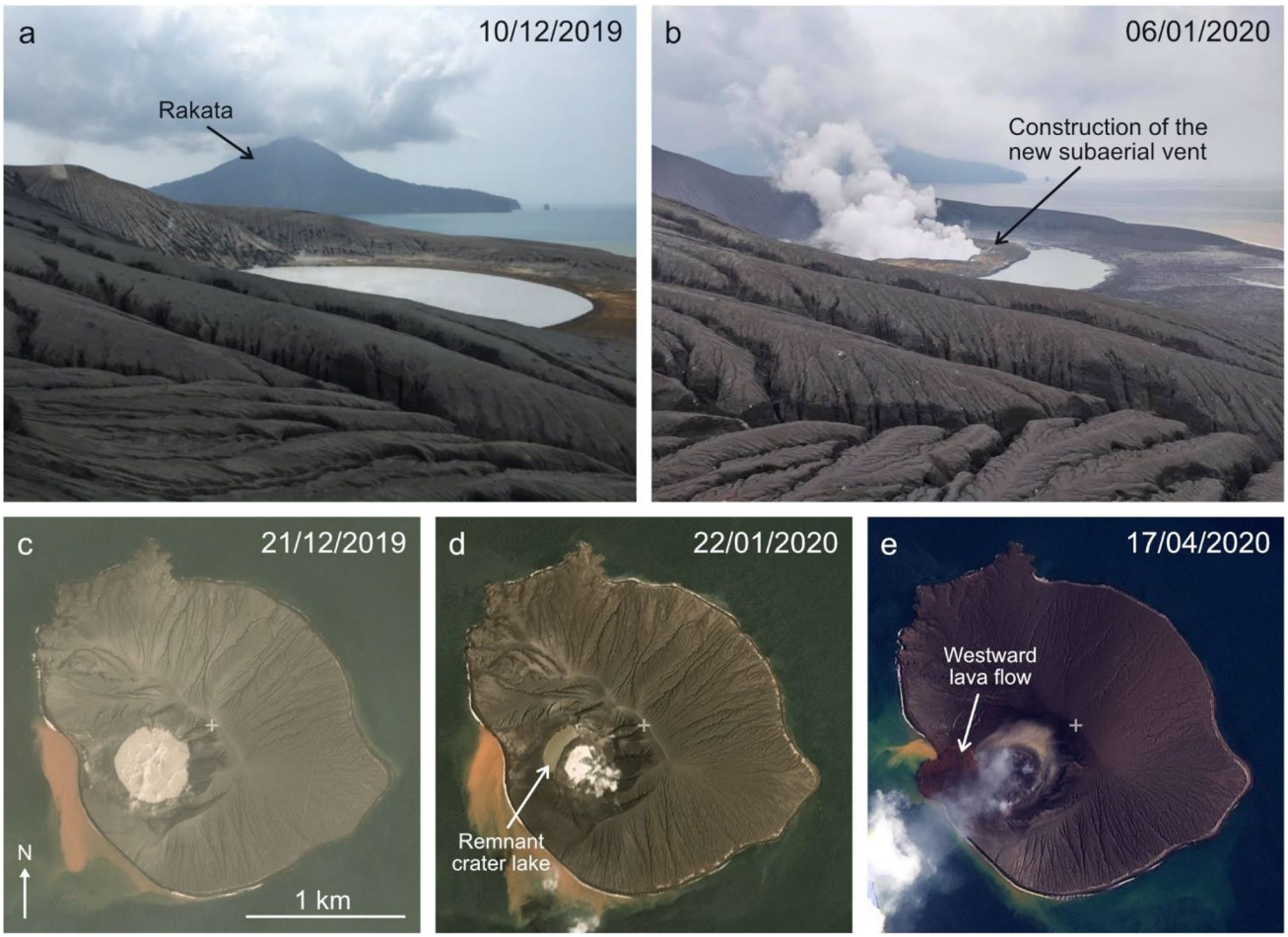

Fig. 8 Stage 5: Development of the post-collapse pyroclastic cone and subsequent lava flows, between December 2019 and April 2020. **a** No cone (Smieszek 2019) and **b** new subaerial cone (Rendezvous 2020) are taken from approximately the same location, north of the crater lake and facing southward, approximately 1 month apart. **c–e** PlanetScope images (all of the same area and at the same scale) from 21 December 2019 (**c**; no cone), 22 January 2020 (**d**; new subaerial cone and partially infilled lake), and 17 April 2020 (**e**; reinitiation of lava flows). The + at the centre of each satellite image (corresponding to the eastern rim of the buried tuff cone) is at 6.09963°S 105.42583°E

in satellite imagery on 23 April 2022, further expanding the western coastline.

By June 2023, Anak Krakatau's subaerial volume totalled 0.156 km^3 (Fig. 4), an increase of 22.9% from August 2019. Of this growth, 66.5% occurred in the SW sector, reversing the December 2018 to August 2019 growth pattern, and more closely replicating the post-1960 development. As of June 2023, the 2020 and 2022 lavas collectively reached up to 50 m in thickness and extended up to 850 m (subaerially) from the central vent. Vent height continued to increase, reaching 103 m by 12 June 2023, whilst maximum island height showed more limited growth (via tephra deposition), increasing to 164 m (Fig. 4b).

When accounting for erosion, the reconstructed subaerial volumetric growth rate from August 2019 to June 2023 was 0.0085 km^3/year (non-erosion corrected, 0.0076 km^3/year). The SW sector of the edifice accounted for 21.6% of the total island volume and 26.7% of the surface area.

Total growth (submarine and subaerial)

Although extremely limited, bathymetric data from 1919, 1990 and 2019 are still sufficient to demonstrate that the major proportion of Anak Krakatau's erupted products form submarine rather than subaerial deposits.

Despite the SW sector's minimal early *subaerial* development, with essentially no permanent growth until lava flows were established in 1960–63, erupted material was still accumulating on both the submerged caldera scarp and caldera floor. By 1990, this material had built out the submerged base of the edifice by 600–700 m to the SW, relative to the position of the 1919 caldera scarp, whilst maintaining the steep ~24° gradient (Fig. 9). We estimate that most of this outward growth occurred by the late 1930s to early 1940s and was equivalent to the material that rapidly accumulated above sea level on the NE side. This is inferred from the subaerial extent of the SW flank from the 1930s onward (Fig. 9); for tuffs to temporarily accumulate and then erode (Fig. 6), and for subsequent lava deltas to remain emergent at the surface, the submarine flank must have built sufficiently outward. Using the difference between the 1919 and 1990 bathymetry (and the 1990 reconstructed DEM), we estimate that ~70% of the total erupted volume between 1927 and 1990 was ultimately deposited as submarine material (either directly or via island erosion). After 1990, growth of the submerged SW flank cannot be well constrained. However, expansion of the SW coastline during this period was minor, resulting primarily from lava flows in 1992–1993 and 2012 (Abdurrachman et al. 2018). It is therefore unlikely that the submarine morphology changed significantly from 1990 to the point of collapse in 2018.

The 2018 collapse and subsequent intense regrowth altered the geometry of the SW submarine flank considerably. Rapid burial obscured the precise submarine failure geometry and extended the submarine edifice. As of August 2019, the SW submarine slope gradient was reduced to ~16°, and the edifice base extended by 250–300 m on the SW side (Fig. 9). The collapse itself carried a substantial volume (~0.116 km^3) of previously subaerial material offshore, whilst the vigorous post-collapse activity also led to extensive submarine deposition, draping the submarine deposits in many metres of material (Hunt et al. 2021). These processes mean that since the collapse, an even greater proportion (increasing from ~70% as of 1990 to > 77% in 2019) of Anak Krakatau's total erupted volume of 1.29 km^3 (1927–2019) now form submarine, rather than subaerial, deposits. This is based on the difference between the 1919 and 2019 bathymetry (combined with the subaerial drone-derived DEM from 2019). Without more recent bathymetric data, we are unable to determine the island's current submarine morphology,

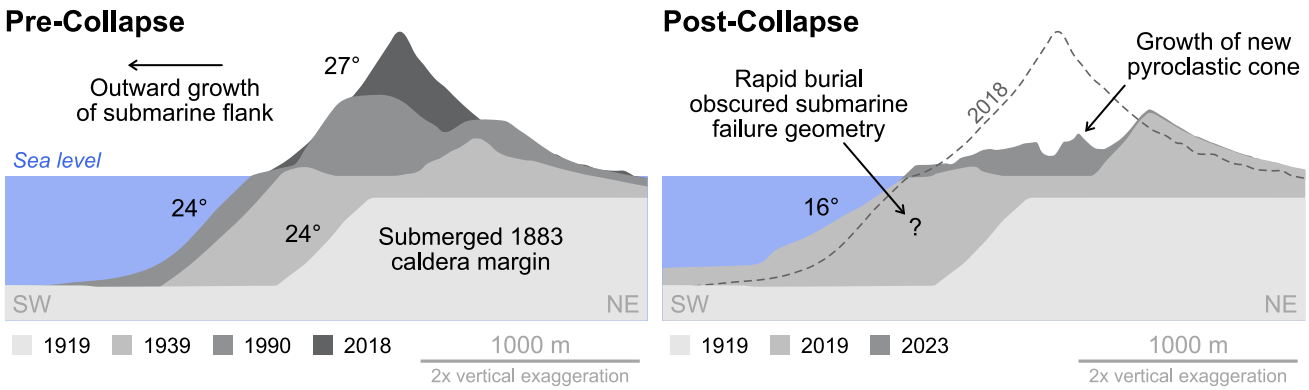

Fig. 9 Schematic cross section (extended SW–NE transect from Fig. 3) of Anak Krakatau's submarine development. Pre-collapse, the SW flank extended progressively outwards from the submerged caldera scarp, broadly maintaining a similar slope angle (~24°). The submarine slope is calculated from bathymetric surveys conducted in 1919 (Escher 1919; Stehn 1929b) and 1990 (Deplus et al. 1995), but is inferred for 1939 based on the island's subaerial extent. Post-collapse, the submarine collapse scar was rapidly buried, obscuring the precise failure geometry, and reducing the slope angle to ~16°. 2019 bathymetry from (Hunt et al. 2021)

particularly relating to the emplacement of the 2020 and 2022 lava flows, and their submarine extent.

Discussion

Although the majority of Anak Krakatau's erupted volume lies offshore, the subaerial growth rates derived here offer a high-resolution insight into relative eruption rates and edifice growth. They show consistent trends between phreatomagmatic and purely magmatic phases of activity and can be used to evaluate loading of the unstable SW flank. These rates can also be projected to assess Anak Krakatau's future growth trajectory, although a full evaluation of flank stability must also account for the morphology of the submerged flank, requiring bathymetric surveying.

The post-collapse regrowth of Anak Krakatau shares many morphological similarities to its 1950s–1960s development. During both intervals, the island's overall structure was strongly asymmetrical, with the buried tuff cone wall (east of the active vent) forming a prominent amphitheatre-shaped high (up to 164 m in 2023 and 167 m in 1963; Fig. 10). The NE flank sloped gently towards the coast, at an average gradient of ~11° (2023) and ~14° (1963), whilst the inner slope dipped towards the active cone at ~23° and ~38° (measured across a SW–NE transect; Fig. 10). Both intervals also saw the relatively rapid development of a new central pyroclastic cone, dissecting and then infilling the crater lake, with vent height increasing at ~30 m/year (2019–2023) and ~32 m/year (1959–1963).

However, the erosion corrected volumetric growth rate for 2019–2023 is substantially higher (0.0084 km^3/year) than that from 1953 to 1963 (0.0037 km^3/year), suggesting a more rapid post-collapse magma flux to the surface, and a greater rate of flank loading than in the 1960s. Whether this accelerated rate will be maintained is uncertain; actively monitoring future growth is therefore essential in understanding if and when the SW flank will reach a slope gradient comparable to the 2018 instability conditions. The pre-collapse (1960–2018) subaerial growth rate was relatively steady and focused on the SW sector of the island. It is possible that the current (2019–2023) higher growth rate is an ongoing response to magma system depressurisation and temporarily enhanced eruption rates following the 2018 collapse (Cutler et al. 2022). Future growth rates may therefore be likely to gradually decline to rates closer to the long-term 1960–2018 average.

Projecting future instability

The 2018 Anak Krakatau collapse occurred without recognised warning. A network of multi-parameter monitoring stations, including digital cameras, differential GPS and seismometers, were installed on Anak Krakatau (Hoffman-Rothe et al. 2006; Hochfeld et al. 2022), but a protocol for systematically monitoring flank stability (rather than magmatic eruptive activity) was not in place. Nevertheless, earlier assessments had indicated potential flank instability on the SW side (Giachetti et al. 2012) and reported concurrent flank subsidence (Agustan et al. 2012; Chaussard and Amelung 2012). Retrospective investigations using multi-temporal InSAR data showed gradual seaward movement of the SW flank for at least four years prior to collapse (Zorn et al. 2023; Kim et al. 2024). Sliding velocities accelerated in late January 2017 and again in June 2018, both coinciding with elevated thermal emissions characteristic of short-lived magmatic intrusions (Walter et al. 2019; Zorn et al. 2023). Although evident now, these signs of instability were not recognised at the time, and the alert level was not raised. However, importantly, they imply that incipient flank movement may be identifiable over a several-year timescale prior to collapse, at least in the context of small volcanic islands, like Anak Krakatau. If flank monitoring can be combined with an evaluation of when the edifice may approach a point of critical instability, by projecting future growth trajectories and calibrating these against the 2018 failure conditions, then this forms a potential basis for managing future instability hazards.

The 2018 lateral collapse was ultimately a consequence of Anak Krakatau's inherent structural asymmetry, stemming from the volcano's formation on the submerged 1883 caldera scarp (Fig. 9). The pre-collapse island additionally contained an intrinsic structural discontinuity: the submarine and basal portions of the edifice consist of tuffs and volcaniclastic material, erupted during the early phreatomagmatic phases, and are overlain by the denser post-1960 pyroclastic cone and lavas (Fig. 3). This boundary itself is inclined to the SW, due to the asymmetry of the tuff cone, and is likely to result in a permeability contrast that may focus hydrothermal fluid flow, pore-fluid pressurisation and alteration. Together, these features generate a deep-seated plane of weakness within the edifice (Stoepke et al. 2025). The correlation between the 2018 collapse scar and the morphology of the pre-1960 tuff cone crater wall, including the scar's wide opening angle, suggests that the internal lithological discontinuity at Anak Krakatau strongly influenced the 2018 failure plane and sliding surface, and therefore also controlled the landslide volume and tsunami magnitude. The structural asymmetry and internal lithological discontinuity persist in the post-2018 edifice, suggesting that future instability, driven by similar processes, is possible.

With each renewed eruptive phase, Anak Krakatau continues to grow. Our work provides the foundation to understand loading of the 2018 failure surface and to define the conditions at which this structure became critically unstable. Any future point of critical instability may be modified

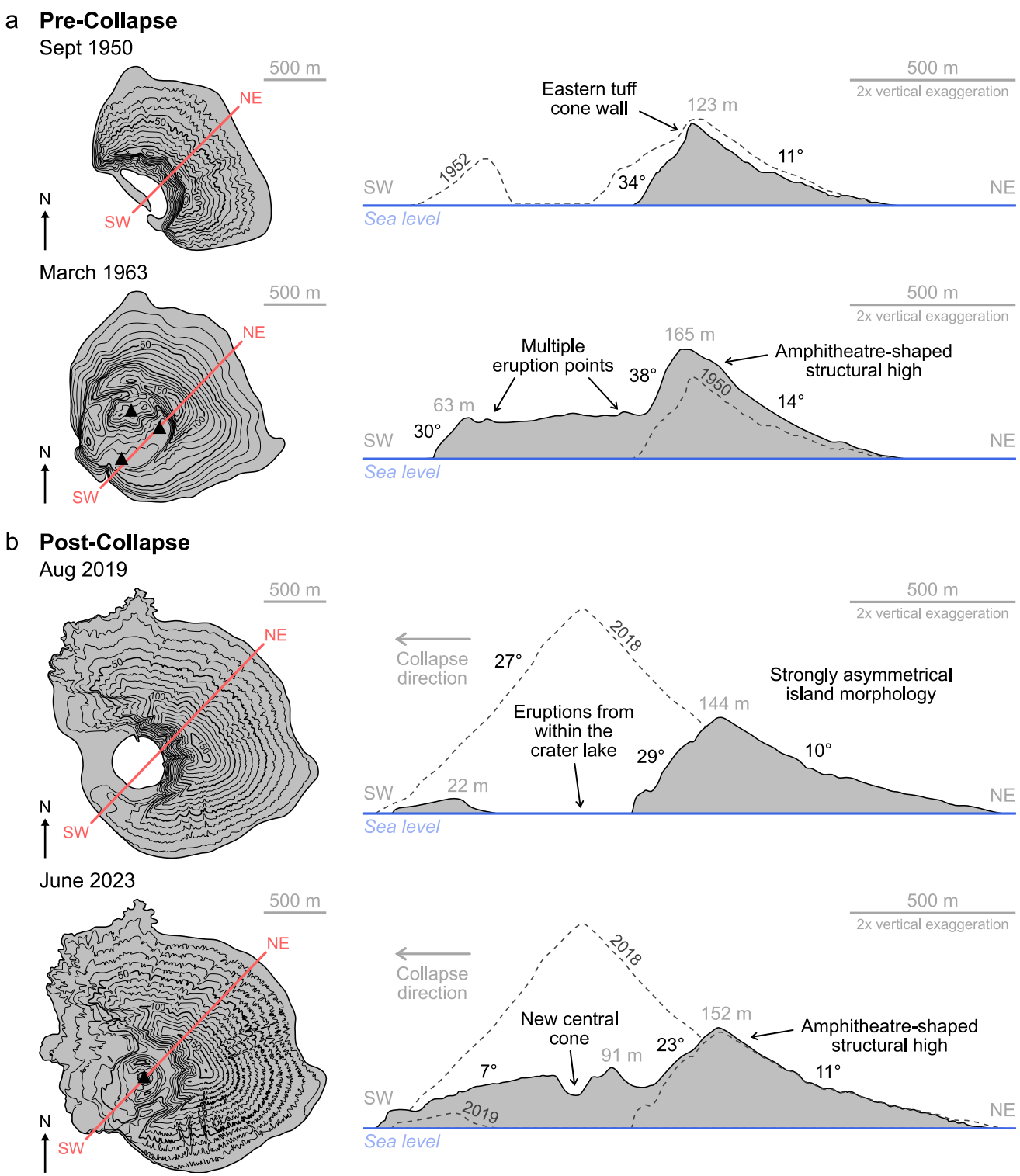

Fig. 10 Anak Krakatau's post-collapse regrowth closely replicates the historical development pattern observed between 1950 and 1963. During both periods the pyroclastic cone, and subsequent early lava flows, were confined to the SW sector of the island due to the pre-existing topography (e.g. the high tuff cone wall). **a** Pre-collapse: reconstructed topography and SW–NE profiles from September 1950 (based on Decker and Hadikusumo 1961) and March 1963 (based on Zen and Hadikusumo 1964). **b** Post-collapse: drone-derived topography and SW–NE profiles from August 2019 and June 2023. All contours are at 10 m intervals, black triangles denote subaerial vents; all profiles follow the SW collapse direction, cutting through the centre of the 2023 pyroclastic cone

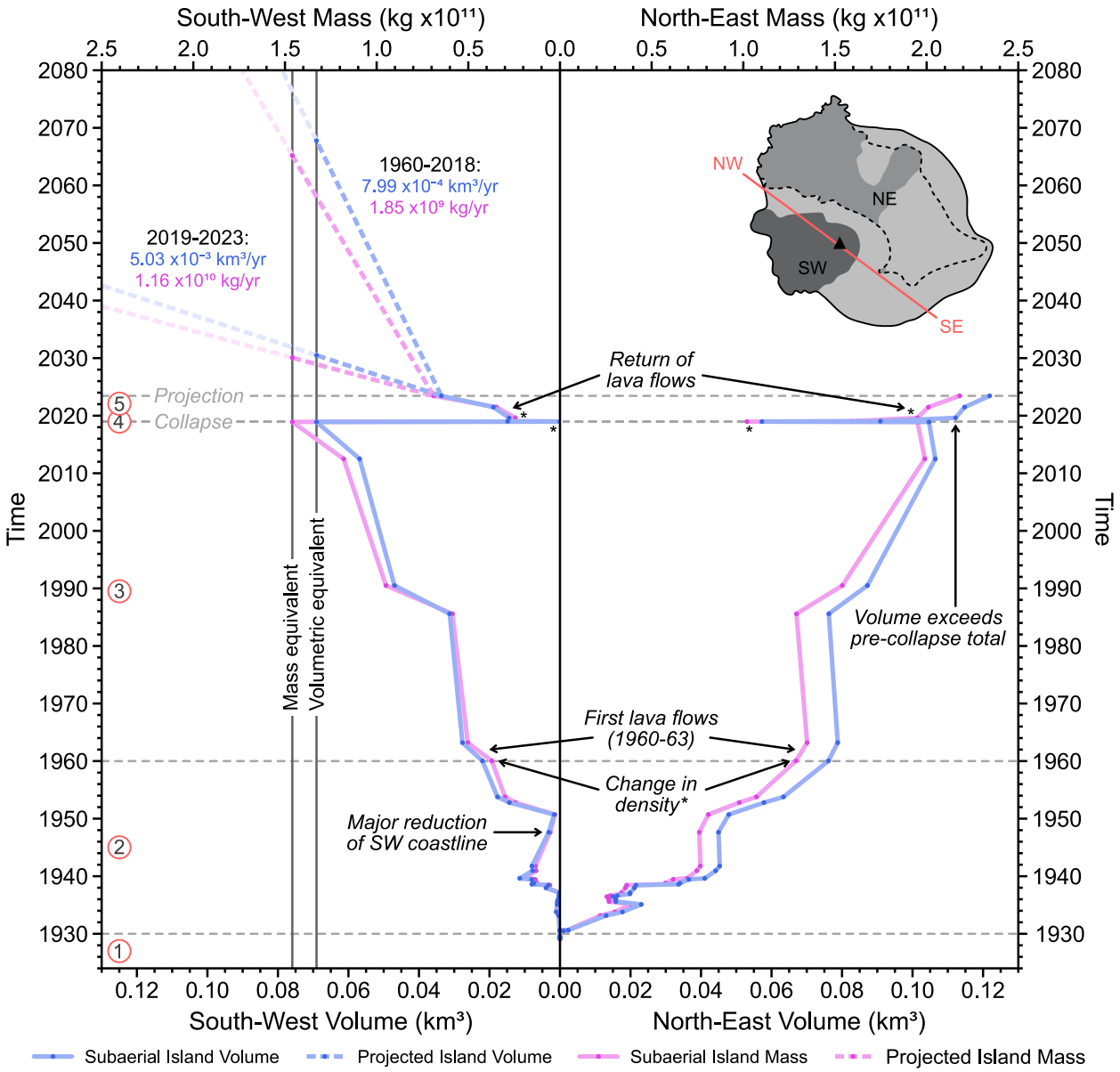

Fig. 11 Anak Krakatau's subaerial loading across the SW and NE sectors of the island (1929–2023). The sectors are defined parallel to the collapse orientation, cutting through the active vent, which is marked by the black triangle (inset map; 2023 island morphology). Projected future volumetric growth and mass trajectories are estimated based on two scenarios: (1) growth continuing at rates observed between 2019 and 2023 and (2) growth slowing to historical rates observed between 1960 and 2018. Red circled numbers refer to development stages discussed throughout. For clarity, mass loading is just shown using the 2.315 g/cm^3 lava density value. Although a lower density would reduce the absolute mass loading values, it has only a minor effect on projected 2018-equivalent loading timescales (Table 3)

relative to the 2018 point of failure by factors including the submarine flank gradient and the extent of subsurface alteration and fluid pressurisation. Nevertheless, past and current growth rates allow the current condition of Anak Krakatau to be placed into a long-term context, to understand when the future edifice may reach conditions comparable to 2018, both in absolute terms (i.e. equivalent volume and mass loading of the SW sector) and, perhaps more importantly, in relative morphological terms (i.e. reaching a comparable subaerial gradient to the 2018 pre-collapse cone). This places constraints on the timing of potential instability, which should be evaluated alongside monitoring of flank movement and other indicators of subsurface conditions (e.g. hydrothermal activity).

As of June 2023, the subaerial portion of the edifice totalled 0.156 km^3, which is approximately 90% of its 2018

pre-collapse volume. When compared to the pre-2018 historical edifice development, this is an extraordinary rate of regrowth, raising concerns over the timeframe and scale of potential destabilisation, alongside the preparedness for future hazards. However, the edifice is broader than it was in 2018 and still well below the 2018 slope gradient (Fig. 10), with much of the recent regrowth including mass accumulated on the stable NE side. As noted above, the 2019–2023 growth rate is also not representative of longer-term (pre-collapse) averages and may slow, highlighting the importance of systematic drone surveying to track edifice development. To understand the timescale in which Anak Krakatau may reach its former pre-collapse thresholds, we project two growth scenarios, focusing on the unstable SW flank (using the same NW–SE alignment referred to throughout this paper). Prior to collapse, the SW island sector totalled 0.069 km^3 (Fig. 11); as of June 2023, this same sector totals 0.034 km^3 (~49% of its pre-collapse volume).

If growth continues at the 2019–2023 rates, the SW flank is projected to reach the 2018 *volumetric* and *mass* thresholds by ~2030 (Fig. 11; Table 3). This is regardless of the selected lava density values, since this projection is not strongly dependent on the absolute density estimate. However, this projection may not be a realistic representation of future instability risk for two reasons. The first is that the long-term future growth rate is likely to decrease, particularly given the current pause in eruptive activity (since late 2023) and the long-term pre-collapse trends. The 1960–2018 growth rate (a period consistent with the current eruptive style at Anak Krakatau) may therefore be a better representation of future edifice development. Projecting the 1960–2018 growth rate implies that the SW flank would reach failure conditions equivalent to 2018 by 2065–2066 (mass) to 2068 (volume) (Table 3). The second reason is that the edifice's basal area is larger than in 2018, and it may therefore be more valid to project an equivalent morphology (i.e. slope gradient) to the 2018 collapse conditions, rather than simply consider the absolute edifice volume or mass. Currently, the volcano's subaerial profile is far lower than in 2018; pre-collapse, the SW flank had a subaerial gradient of ~27° (Fig. 10b), but as of June 2023, the slope angle was just ~7° along the same transect (Fig. 10b). The 2023 SW coastline also now extends an additional ~25 m further offshore, in the direction of failure, relative to the 2018 pre-collapse edifice. Using this basal distance (706 m; calculated from the shore to the central vent) and the pre-collapse slope angle of 27°, we estimate that Anak Krakatau will approach an equivalent slope gradient at ~360 m in height. This is approximately 30 m higher than the 2018 point of failure. Any further increases in island diameter would increase this equivalent edifice height, and therefore also increase the projected potential failure volume (see discussion in Online Resource 3). By approximating the shape of this future edifice load on the SW sector as a simplified half-cone (0.094 km^3) and subtracting the proportion of material already within this shape, based on the 2023 DEM, then the 1960–2018 growth rates imply that a morphologically similar failure condition would be met in ~2104 (Table 3). The 2019–23 volumetric growth rates would lead to this condition being met much sooner, in ~2036. Whilst, as noted above, we do not consider this a likely long-term growth rate, this does nevertheless highlight the importance of ongoing measurements of edifice growth at Anak Krakatau to refine these projections over the coming decades.

Given the increased post-2018 island diameter, if a future collapse occurred with a similar geometry to the 2018 failure, and was controlled by a similar failure plane, it would have a larger volume than the 2018 event (an increase of ~40% is implied by the SW sector morphologic equivalent dimensions; Table S3.4). Further increases in island

Table 3 Summary of current (2019–2023) and historical (1960–2018) subaerial growth rates (volume and mass) of Anak Krakatau's SW sector, including the timeframe in which each parameter is projected to reach the estimated collapse threshold

SW sector	Current regrowth rate (2019–2023)	Historical growth rate (1960–2018)
Volume	5.03×10^{-3} km^3/year	7.99×10^{-4} km^3/year
Mass *(upper bound, density of 2.315 g/cm^3)*	1.16×10^{10} kg/year	1.85×10^{9} kg/year
Mass *(lower bound, density of 2.08 g/cm^3)*	1.05×10^{10} kg/year	1.66×10^{9} kg/year
Point of reaching comparable pre-collapse *volume*	2030	2068
Point of reaching comparable pre-collapse *mass* (upper bound, density of 2.315 g/cm^3)*	2030	2065
Point of reaching comparable pre-collapse *mass* (lower bound, density of 2.08 g/cm^3)*	2030	2066
Point of reaching comparable pre-collapse *morphology***	2036	2104

*This assumes that the projected emplaced mass is lava

**This assumes all subsequent growth on the SW flank accumulates as a cone with a 27° flank gradient, rather than accumulating as lava flows beyond the footprint of this cone

diameter on the SW side would correspondingly increase the estimated time at which failure conditions may be met (assuming equivalent morphology to the 2018 failure) and the volume of that failure. We additionally emphasise that future failure conditions are also subject to various other uncertainties, and the reduced gradient of the submarine flank is likely to be particularly important as a relative stabilising factor, which would push our projected timings of instability further into the future. The timescale and extent of alteration within the edifice are also likely to influence future collapse timings. For the 2018 collapse, subsurface rock properties were influenced by up to 90 years of potential alteration; in the present-day edifice, the post-2018 rocks are currently likely to be significantly less altered by hydrothermal activity than equivalent pre-2018 rocks.

Recommendations and future monitoring

Our projections do not necessarily translate to forecasting timescales of future collapse at Anak Krakatau. They instead bracket the period in which the volcano is likely to reach comparable geometries to the 2018 failure, although additional factors including the volcano's altered submarine morphology, characteristics of subsurface structural discontinuities, rock strength and extent of hydrothermal alteration are all likely to influence edifice stability and therefore the scale, geometry and timeframe of future failure. Bathymetric surveys and detailed characterisation of internal rock properties, alongside tracking of future growth rates (as shown here) and monitoring of flank movement, should all be undertaken to comprehensively assess future edifice stability.

Following the 2018 collapse, the gradient of Anak Krakatau's submarine SW flank was reduced by ~8° and the base extended outward by 250–300 m (Fig. 9). The failure additionally emplaced a thick (up to 70 m in places) blocky deposit across the caldera floor, covering an area of 7.2 km^2 SW of Anak Krakatau (Hunt et al. 2021), which is likely to act as a reinforcement to the newly extended submarine flank. These combined factors likely extend any future failure further into the future, but would also imply a correspondingly larger potential failure volume if the SW flank becomes unstable.

Hydrothermal alteration is a key controlling factor in edifice destabilisation (e.g. Reid et al. 2001; Reid 2004; Romero et al. 2021). The level of alteration occurring within Anak Krakatau is not well constrained. No major zones of superficial alteration are visible in our 2023 drone survey, nor within samples from surface deposits used for measuring density. Novellino et al. (2020) note higher Normalised Difference in Water Index (NDWI) observed in Sentinel 2 Level-1C satellite imagery around the crater and crater walls, potentially reflecting hydrothermal alteration or a possible shadowing effect. At Surtsey volcano, boreholes through the edifice (including the submarine portion) revealed the physical properties of the pyroclastic deposits to be highly heterogeneous, becoming progressively more altered with depth (increase in nanocrystalline clay minerals) (Jakobsson and Moore 1986; Jackson et al. 2019, 2024). Alteration associated with the formation of clays can reduce volcanic rock strength, lowering the friction coefficient and promoting instability (John et al. 2008; Heap et al. 2021). If Anak Krakatau's deposits are similarly altered, the edifice may be further preconditioned to future failure. The internal boundary between tuffs and lavas may additionally act as a pathway for hydrothermal fluids, alteration, and a weakened failure plane (Stoepke et al. 2025). An improved understanding of Anak Krakatau's internal rock properties is therefore critical in evaluating the mechanics and timeframe of future potential failure events.

Since the 2018 collapse, a new emergency system based on the Inexpensive Device for Sea Level monitoring (IDSL) has been implemented within the Sunda Strait. It uses a network of fast response tide gauges to transmit real-time monitoring of sea levels. Any detected abnormal waves are sent for human verification, and if confirmed will activate coastal warning sirens (Annunziato et al. 2019). The first devices were installed in January 2019 at Sebesi Island and Marina Jambu (Banten), approximately ~18 km NNE and ~46 km E of the volcano (Annunziato et al. 2019). The locations of these were limited by the availability of cellular networks. However, the development of a dedicated satellite system enabled the installation of an additional IDSL at Rakata Island in May 2022 (GDACS 2022). Whilst this system provides an updated protocol to both detect and communicate risk of an impending volcanic or landslide-generated tsunami, the window for safely evacuating residents is limited by the short tsunami travel time, which is ~30–40 min for the populated areas within ~50 km from Anak Krakatau. Improved recognition and monitoring of pre-failure conditions is therefore imperative in successfully enacting management plans, timely evacuations and temporary relocations.

The use of regular repeated drone mapping can offer a relatively inexpensive and time-efficient route to providing snapshots of edifice development to build on the dataset assembled here. With clear weather conditions and low eruptive activity, a complete survey on Anak Krakatau takes only 1–2 days. Updated DEMs can then be reviewed in the context of historical growth (Figs. 5, 6, 7, 8, 9 and 10), both to evaluate the progression of edifice growth, updating future projections if necessary, but also to identify when the volcano begins to approach the slope gradient of the 2018 collapse. This is then a point where targeted measurements of flank movement, particularly to detect any movement acceleration (with the potential to deploy both ground-based and satellite (e.g. InSAR) methods), will become critical in identifying signals which may precede collapse.

Conclusion

The lateral collapse of volcanoes presents a major and often cascading series of hazards, particularly in island settings where the generation of tsunamis has potentially far-reaching consequences. However, as gravity-driven processes conditioned by various short- and long-timescale factors, such events are challenging to forecast and the signals preceding flank collapse may not easily be recognised via standard volcano monitoring methods, as exemplified by Anak Krakatau's 2018 failure. The ability to identify the timing, precursory indicators and magnitude of collapses is essential for effective volcanic risk management. By integrating Anak Krakatau's eruptive history and structural development (both pre- and post-collapse), we are able to evaluate future growth and stability trajectories, aiding the recognition of future instability risks and potential collapse precursors.

1. Anak Krakatau's pre-collapse eruptive history consisted of three main temporal phases: the initiation of volcanism (1927–1930), a phreatomagmatic phase (1930–1960) and transition to Strombolian-dominated activity thereafter (1960–2018). Each of these shifts corresponded to key developments in the island's morphology, principally the transition from a submerged vent to rapid construction of the pyroclastic cone around 1960.
2. Anak Krakatau was constructed on the edge of the 1883 Krakatau caldera scarp, imparting an inherent asymmetry from its earliest development. The 1960 transition in eruptive behaviour produced a lithological discontinuity on this asymmetrical surface, separating pre-1960 tuffs from post-1960 lavas. This boundary closely coincides with the 2018 failure plane and strongly influenced the collapse geometry. This structure persists in the post-2018 edifice and is likely to control future instability.
3. The 2018 lateral collapse removed all subaerial material from the SW sector of the volcano, including the summit region, returning the vent to below sea level and reducing the island's surface area by 46.7% and subaerial volume by 67.0%—a total subaerial volume loss of 0.116 km^3.
4. Anak Krakatau's post-collapse regrowth has followed a similar development cycle to its pre-collapse history, but on an extremely accelerated scale. After an initial period of very rapid post-collapse regrowth (producing the equivalent of 10 years of pre-collapse growth in 19 days), the eruption rate has remained high, with the 2019–2023 volumetric growth being 4.7 times the long-term pre-collapse (1960–2018) average. Whether this will be sustained is uncertain, but it calls into question the timeframe of potential future destabilisation and highlights the need for ongoing monitoring and preparedness for future hazards.
5. With continued regrowth, the edifice may approach a future point of critical instability. By projecting the 2019–2023 growth rates and assuming a simple conical form accumulating on the current SW flank, a morphology (i.e. slope gradient) comparable to the 2018 failure could be met by ~2036. A decline in growth rates to the 1960–2018 average would imply this threshold could instead be reached by 2104 (or beyond, if there is further increase in the island radius on the SW side). Future growth to a morphological equivalent of the 2018 failure conditions also implies a potentially larger collapse volume, increasing by 40% compared to 2018, if a similar failure geometry is assumed. However, subaerial edifice morphology is not the only factor likely to control future stability: the gradient and stability of the submarine flank, in addition to internal alteration and physical properties, are all likely to be important, and should be evaluated collectively as part of future monitoring strategies.
6. Implementing regular drone surveys and satellite-based remote sensing of Anak Krakatau could provide a low-cost, time-efficient method to monitor future edifice development and track the growth trajectories presented here, particularly in providing an early indication of when the volcano approaches similar dimensions to the 2018 collapse conditions.

Supplementary Information The online version contains supplementary material available at https://doi.org/10.1007/s00445-026-01974-w.

Acknowledgements Indonesian fieldwork was conducted under permit 260/SIP/IV/FR/5/2023. We thank the Balai Konservasi Sumber Daya Alam (BKSDA), the Menteri Energi dan Sumber Daya Mineral (ESDM) and colleagues at BRIN and ITB for their crucial support in completing this fieldwork. KM was supported by NERC CENTA2 grant NE/S007350/1, and SW, MC and SE by NERC grants NE/T002026/1 and NE/S003509/1. MA was supported by PPMI FITB Program from the Faculty of Earth Sciences and Technology Research Scheme. We thank Wayan Indra Saputra for support in collecting the 2019 DEM. We are also grateful to Pablo Tierz, M. Coombs and one anonymous reviewer for their constructive feedback, which helped to improve this manuscript.

Author contributions KM, SW, MC and SE conceptualised the study; KM collated all archival datasets, building on prior resources compiled by SE; KM developed the methods and reconstructed historical topography. KM, SW, AFS and MEN collected field datasets in 2023 with support from MH, DN and MA; AFS and MEN acquired and processed the 2023 drone photogrammetry; additional DEMs were provided by MH and WB. KM and SW led interpretations; KM wrote the initial draft with editing from SW and input from MC, VS, CMP and CS. All authors contributed to the final draft, including analysis and implications.

Funding KM was supported by NERC CENTA2 grant NE/S007350/1, and SW, MC and SE by NERC grants NE/T002026/1 and NE/S003509/1. MA was supported by PPMI FITB Program from the Faculty of Earth Sciences and Technology Research Scheme. We thank Wayan Indra Saputra for support in collecting the 2019 DEM.

We are also grateful to Pablo Tierz, M. Coombs and one anonymous reviewer for their constructive feedback, which helped to improve this manuscript.

Data availability All data presented within this work are provided as online resources (1–4). All reconstructed Digital Elevation Models (DEMs), post-collapse drone-derived DEMs and orthomosaics are provided in a downloadable format here: https://doi.org/10.5281/zenodo.17284993.

Declarations

Competing interests The authors declare no competing interests.

References

Abdurrachman M, Widiyantoro S, Priadi B, Ismail T (2018) Geochemistry and structure of Krakatoa Volcano in the Sunda Strait, Indonesia. Geosciences 8(4):111. https://doi.org/10.3390/geosciences8040111

Agustan, Kimata F, Pamitro YE, Abidin HZ (2012) Understanding the 2007–2008 eruption of Anak Krakatau Volcano by combining remote sensing technique and seismic data. Int J Appl Earth Obs Geoinf 14(1):73–82. https://doi.org/10.1016/j.jag.2011.08.011

Annunziato A, Prasetya G, Husrin S (2019) Anak Krakatau volcano emergency tsunami early warning system. Sci Tsunami Hazards 38(2):68–95

Anon (1915) Vulkanische verschijnselen en aardbevingen in den Oost-Indischen Archipel waargenomen gedurende het jaar 1913. Natuurkundig Tijdschrift Voor Nederlandsch-Indië 75:67–80

Badan Informasi Geospasial (BIG) (2012) DEMNAS National DEM [DEM]. https://tanahair.indonesia.go.id/demnas/#/#Info

Camus G, Gourgaud A, Vincent PM (1987) Petrologic evolution of Krakatau (Indonesia): implications for a future activity. J Volcanol Geotherm Res 33(4):299–316. https://doi.org/10.1016/0377-0273(87)90020-5

Chaussard E, Amelung F (2012) Precursory inflation of shallow magma reservoirs at west Sunda volcanoes detected by InSAR. Geophys Res Lett. https://doi.org/10.1029/2012GL053817

Conrad O, Bechtel B, Bock M, Dietrich H, Fischer E, Gerlitz L, Wehberg J, Wichmann V, Böhner J (2015) System for automated geoscientific analyses (SAGA) v. 2.1.4. Geosci Model Dev 8(7):1991–2007. https://doi.org/10.5194/gmd-8-1991-2015

Cutler KS, Watt SFL, Cassidy M, Madden-Nadeau AL, Engwell SL, Abdurrachman M, Nurshal MEM, Tappin DR, Carey SN, Novellino A, Hayer C, Hunt JE, Day SJ, Grilli ST, Kurniawan IA, Kartadinata N (2022) Downward-propagating eruption following vent unloading implies no direct magmatic trigger for the 2018 lateral collapse of Anak Krakatau. Earth Planet Sci Lett 578:117332. https://doi.org/10.1016/j.epsl.2021.117332

De Neve GA (1951) Luchtverkenningen boven de vulkanen van Sumatra, Java en de Kleine Sunda Eilanden. De Ingenieur in Indonesië 3(2):IV.13-IV.22

De Neve GA (1985) Earlier eruptive activities of Krakatau in historic time and during the Quaternary. In LIPI: Proceedings of the Symposium on 100 years development of Krakatau and its surroundings, pp 35–46. Jakarta, 23–27 August, 1983.

Decker RW (1961) Renewed activity of Anak Krakatau. Tulsa Geol Soc Dig 29:117–119

Decker RW, Hadikusumo D (1961) Results of the 1960 expedition to Krakatau. J Geophys Res Space Phys 66(10):3497–3511. https://doi.org/10.1029/JZ066i010p03497

Deplus C, Bonvalot S, Dahrin D, Diament M, Harjono H, Dubois J (1995) Inner structure of the Krakatau volcanic complex (Indonesia) from gravity and bathymetry data. J Volcanol Geotherm Res 64(1):23–52. https://doi.org/10.1016/0377-0273(94)00038-I

Escher BG (1919) Veranderingen in de Krakatau-groep na 1908 en wijzigingen in de opvatting van eenige geologische details. Handelingen van Het Eerste Nederlandsch Indisch Natuurwetenschappelijk Congress, 198–219.

Furneaux R (1964) Krakatoa. Prentice-Hall, Inc. pp. 224

Gardner MF, Troll VR, Gamble JA, Gertisser R, Hart GL, Ellam RM, Harris C, Wolff JA (2013) Crustal differentiation processes at Krakatau Volcano, Indonesia. J Petrol Geol 54(1):149–182. https://doi.org/10.1093/petrology/egs066

GEBCO Bathymetric Compilation Group 2024 (2024) The GEBCO_2024 Grid—a continuous terrain model of the global oceans and land. NERC EDS British Oceanographic Data Centre NOC. https://doi.org/10.5285/1c44ce99-0a0d-5f4f-e063-7086abc0ea0f

Giachetti T, Paris R, Kelfoun K, Ontowirjo B (2012) Tsunami hazard related to a flank collapse of Anak Krakatau Volcano, Sunda Strait, Indonesia. In J. P. Terry & J. Goff (Eds), Natural Hazards in the Asia–Pacific Region: Recent Advances and Emerging Concepts (Vol. 361, p. 0). Geological Society of London. https://doi.org/10.1144/SP361.7

Global Disaster Alert and Coordination System (GDACS) (2022) Installation of the tsunami early warning system for the Anak Krakatau Volcano. https://www.gdacs.org/Public/download.aspx?type=DC&id=228

Gouhier M, Paris R (2019) SO2 and tephra emissions during the December 22, 2018 Anak Krakatau flank-collapse eruption. Volcanica 2(2):91. https://doi.org/10.30909/vol.02.02.91103

Grilli ST, Tappin DR, Carey S, Watt SFL, Ward SN, Grilli AR, Engwell SL, Zhang C, Kirby JT, Schambach L, Muin M (2019) Modelling of the tsunami from the December 22, 2018 lateral collapse of Anak Krakatau volcano in the Sunda Straits, Indonesia. Sci Rep 9(1):11946. https://doi.org/10.1038/s41598-019-48327-6

Grilli ST, Zhang C, Kirby JT, Grilli AR, Tappin DR, Watt SFL, Hunt JE, Novellino A, Engwell S, Nurshal MEM, Abdurrachman M, Cassidy M, Madden-Nadeau AL, Day S (2021) Modeling of the Dec. 22nd 2018 Anak Krakatau volcano lateral collapse and tsunami based on recent field surveys: comparison with observed tsunami impact. Mar Geol 440:106566. https://doi.org/10.1016/j.margeo.2021.106566

Hadikusumo D (1961a) Bulletin of the Volcanological Survey of Indonesia, for the years 1950–57. No. 100

Hadikusumo D (1961b) Photograph of an ash plume erupting from the cone in the summit crater of Anak Krakatau on 2 May 1961 [Photograph]. Global Volcanism Program (GVP-01032). https://volcano.si.edu/gallery/ShowImage.cfm?photo=GVP-01032

Heap MJ, Baumann T, Gilg HA, Kolzenburg S, Ryan AG, Villeneuve M, Russell JK, Kennedy LA, Rosas-Carbajal M, Clynne MA (2021) Hydrothermal alteration can result in pore pressurization

and volcano instability. Geology 49(11):1348–1352. https://doi.org/10.1130/G49063.1

Hedervari P (1986) Catalog of Submarine volcanoes and hydrological phenomena associated with volcanic events, January 1, 1900 to December 31, 1950. National Oceanic and Atmospheric Administration, National Geophysical Data Center, World Data Center A for Solid Earth Geophysics

Hochfeld I, Hort M, Schwalbe E, Dürig T (2022) Eruption dynamics of Anak Krakatau volcano (Indonesia) estimated using photogrammetric methods. Bull Volcanol 84(8):73. https://doi.org/10.1007/s00445-022-01579-z

Hoffman-Rothe A, Ibs-von Seht M, Knieβ R, Faber E, Klinge K, Reichert C, Purbawinata MA, Patria C (2006) Monitoring Anak Krakatau Volcano in Indonesia. Eos Trans Am Geophys Union 87(51):581–586. https://doi.org/10.1029/2006EO510002

Huiskamp B (1950) [Photograph]. X.com (profile @WHuiskamp). https://x.com/whuiskamp/status/1248971711187423245?s=46

Hunt JE, Tappin DR, Watt SFL, Susilohadi S, Novellino A, Ebmeier SK, Cassidy M, Engwell SL, Grilli ST, Hanif M, Priyanto WS, Clare MA, Abdurrachman M, Udrekh U (2021) Submarine landslide megablocks show half of Anak Krakatau island failed on December 22nd, 2018. Nat Commun 12(1):2827. https://doi.org/10.1038/s41467-021-22610-5

Jackson MD, Gudmundsson MT, Weisenberger TB, Rhodes JM, Stefánsson A, Kleine BI, Lippert PC, Marquardt JM, Reynolds HI, Kück J, Marteinsson VT, Vannier P, Bach W, Barich A, Bergsten P, Bryce JG, Cappelletti P, Couper S, Fahnestock MF, Zimanowski B (2019) SUSTAIN drilling at Surtsey volcano, Iceland, tracks hydrothermal and microbiological interactions in basalt 50 years after eruption. Sci Drill 25:35–46. https://doi.org/10.5194/sd-25-35-2019

Jackson MD, Heap MJ, Vola G, Ardit M, Rhodes JM, Peterson JG, Tamura N, Gudmundsson MT (2024) Material and mechanical properties of young basalt in drill cores from the oceanic island of Surtsey, Iceland. GSA Bull 136(9–10):3527–3552. https://doi.org/10.1130/B37037.1

Jakobsson SP, Moore JG (1986) Hydrothermal minerals and alteration rates at Surtsey volcano, Iceland. GSA Bull 97(5):648–659. https://doi.org/10.1130/0016-7606(1986)97%253C648:HMAARA%253E2.0.CO;2

John DA, Sisson TW, Breit GN, Rye RO, Vallance JW (2008) Characteristics, extent and origin of hydrothermal alteration at Mount Rainier Volcano, Cascades Arc, USA: implications for debris-flow hazards and mineral deposits. J Volcanol Geotherm Res 175(3):289–314. https://doi.org/10.1016/j.jvolgeores.2008.04.004

Judd JW (1888) On the volcanic phenomena of the eruption, and on the nature and distribution of the ejected materials (Part 1). In The Eruption of Krakatoa, and Subsequent Phenomena: Report of the Krakatoa Committee of the Royal Society, pp 1–56. Trübner & Company

Keating BH, McGuire WJ (2000) Island edifice failures and associated tsunami hazards. Pure Appl Geophys 157(6):899–955. https://doi.org/10.1007/s000240050011

Kim YC, Wauthier C, Walter TR (2024) Satellite geodesy uncovers 15 m of slip on a detachment fault prior to the 2018 collapse at Anak Krakatau, Indonesia. Geophys Res Lett 51(22):e2024GL112296. https://doi.org/10.1029/2024GL112296

Koninklijke Nederlandsch–Indische Luchtvaart Maatschappij (KNILM) (1930) Uitbarsting van de Krakatau in 1930. Het kratermeer van de Krakatau [Photograph]. Collectie Stichting Nationaal Museum van Wereldculturen, Netherlands (TM-ALB-1427–212). https://hdl.handle.net/20.500.11840/513183

Koninklijke Nederlandsch–Indische Luchtvaart Maatschappij (KNILM) (1938) Luchtopname. Krakatau [Anak Krakatau] [Photograph]. Fotocollectie Spaarnestad Onderwerpen, Nationaal Archief (505057_012). http://hdl.handle.net/10648/b560dfc4-df53-fbbb-0180-6beaf3e4f8e2

Madden-Nadeau AL, Cassidy M, Pyle DM, Mather TA, Watt SFL, Engwell SL, Abdurrachman M, Nurshal MEM, Tappin DR, Ismail T (2021) The magmatic and eruptive evolution of the 1883 caldera-forming eruption of Krakatau: integrating field- to crystal-scale observations. J Volcanol Geotherm Res 411:107176. https://doi.org/10.1016/j.jvolgeores.2021.107176

Manzella I, Makris S, Casalbore D, Cole P, Kelfoun K, Georgiopoulou A, Hicks A, van Westen C (2024) Cascading hazards in volcanic environments: monitoring, modelling and impact analysis of tsunamigenic flows for risk reduction. Ann Geophys. https://doi.org/10.4401/ag-9191

Moore JG (1985) Structure and eruptive mechanisms at Surtsey Volcano, Iceland. Geol Mag 122(6):649–661. https://doi.org/10.1017/S0016756800032052

Nagahara S, Miyamoto S, Morishima K, Nakano T, Koyama M, Suzuki Y (2022) Three-dimensional density tomography determined from multi-directional muography of the Omuroyama scoria cone, Higashi–Izu monogenetic volcano field, Japan. Bull Volcanol 84(10):94. https://doi.org/10.1007/s00445-022-01596-y

Neumann van Padang M (1933) De Krakatau voorheen en thans. Trop Natuur 22(8):137–150

Neumann van Padang M (1951) Catalogue of the active volcanoes of the world, including solfatara fields: Part 1. International Association of Volcanology, Napoli

Neumann van Padang M (1983) History of the volcanology in the former Netherlands East Indies. Scr Geol 71:1–76

Novellino A, Engwell SL, Grebby S, Day S, Cassidy M, Madden-Nadeau A, Watt S, Pyle D, Abdurrachman M, Edo Marshal Nurshal M, Tappin DR, Andri Kurniawan I, Hunt J (2020) Mapping recent shoreline changes spanning the lateral collapse of Anak Krakatau Volcano, Indonesia. Appl Sci 10(2):536. https://doi.org/10.3390/app10020536

Oddsson B (1982) Rock quality designation and drilling rate correlated with lithology and degree of alteration in volcanic rocks from the 1979 Surtsey drill hole. Surtsey Res Prog Rep 9:94–97

Partomihardjo T, Mirmanto E, Whittaker RJ (1992) Anak Krakatau's vegetation and flora circa 1991, with observations on a decade of development and change. GeoJournal 28(2):233–248. https://doi.org/10.1007/BF00177238

Perttu A, Caudron C, Assink JD, Metz D, Tailpied D, Perttu B, Hibert C, Nurfiani D, Pilger C, Muzli M, Fee D, Andersen OL, Taisne B (2020) Reconstruction of the 2018 tsunamigenic flank collapse and eruptive activity at Anak Krakatau based on eyewitness reports, seismo-acoustic and satellite observations. Earth Planet Sci Lett 541:116268. https://doi.org/10.1016/j.epsl.2020.116268

Petruschevsky VA (1947). Anak Krakatau,1947 [Photograph]. Vladimir Petrushevsky, an archive. https://blogs.dickinson.edu/vapetrushevsky/

Pinel V, Jaupart C, Albino F (2010) On the relationship between cycles of eruptive activity and growth of a volcanic edifice. J Volcanol Geotherm Res 194(4):150–164. https://doi.org/10.1016/j.jvolgeores.2010.05.006

Priyanto WS, Hunt JE, Hanif M, Tappin DR, Permana H, Susilohadi Cassidy M, Yulianto E (2021) Bathymetry and shallow seismic imaging of the 2018 flank collapse of Anak Krakatau. Front Earth Sci, 8. https://doi.org/10.3389/feart.2020.577448

QGIS.org. (2026) QGIS Geographic Information System [Computer software]. QGIS Association. http://www.qgis.org

Reid ME (2004) Massive collapse of volcano edifices triggered by hydrothermal pressurization. Geology 32(5):373–376. https://doi.org/10.1130/G20300.1

Reid ME, Sisson TW, Brien DL (2001) Volcano collapse promoted by hydrothermal alteration and edifice shape, Mount Rainier, Washington. Geology 29(9):779–782. https://doi.

org/10.1130/0091-7613(2001)029%253C0779:VCPBHA%253E2.0.CO;2
Rendezvous P (2020) [Photograph]. Facebook.com (profile @peter.rendezvous.9). https://www.facebook.com/share/1BGbu8mktX/?mibextid=WC7FNe
Global Volcanism Program (1993) Report on Krakatau (Indonesia). Bulletin of the Global Volcanism Network, 18(5). https://doi.org/10.5479/si.GVP.BGVN199305-262000
Global Volcanism Program (2023) Report on Krakatau (Indonesia). Bulletin of the Global Volcanism Network, 48(7). https://volcano.si.edu/showreport.cfm?doi=10.5479/si.GVP.BGVN202307-262000
Romero JE, Polacci M, Watt S, Kitamura S, Tormey D, Sielfeld G, Arzilli F, La Spina G, Franco L, Burton M, Polanco E (2021) Volcanic lateral collapse processes in mafic arc edifices: a review of their driving processes, types and consequences. Front Earth Sci. https://doi.org/10.3389/feart.2021.639825
Roverato M, Di Traglia F, Procter J, Paguican E, Dufresne A (2021) Factors contributing to volcano lateral collapse. In M. Roverato, A. Dufresne, & J. Procter (Eds), Volcanic Debris Avalanches: From Collapse to Hazard, pp 91–119. Springer International Publishing. https://doi.org/10.1007/978-3-030-57411-6_5
Self S (1992) Krakatau revisited: the course of events and interpretation of the 1883 eruption. GeoJournal 28(2):109–121. https://doi.org/10.1007/BF00177223
Siebert L (2002) Landslides resulting from structural failure of volcanoes. In S. G. Evans & J. V. Degraff (Eds), Catastrophic Landslides: Effects, Occurrence, and Mechanisms: XV, (p. 0). Geological Society of America. https://doi.org/10.1130/REG15-p209
Sigurdsson H, Carey S, Mandeville C, Bronto S (1991) Pyroclastic flows of the 1883 Krakatau eruption. Eos Trans Am Geophys Union 72(36):377–381. https://doi.org/10.1029/90EO00286
Smieszek P (2019) [Graphic]. X.com (profile @piotr_smieszek). https://twitter.com/piotr_smieszek/status/1204545970962231296)
Stehn CE (1929a) Krakatau (Lang-Eiland, Verlaten-Eiland). Bulletin of the Netherlands East Indian Volcanological Survey, 20–21
Stehn CE (1929b) Krakatau: the geology and volcanism of the Krakatau group. Proceedings of the Fourth Pacific Science Congress (Batavia)
Stehn CE (1930) Bulletin of the Netherlands India Volcanological Survey, 29–60(35–36)
Stehn CE (1933) Bulletin of the Netherlands Indies Volcanological Survey (Vol. III). Mining and Geological Department, Bandung, 61–74(63)
Stehn CE (1937) Bulletin of the Netherland Indies Volcanological Survey. Mining and Geological Department, Bandung, p 78
Stehn CE (1938) Bulletin of the Netherland Indies Volcanological Survey. Mining and Geological Department, Bandung, p 82
Stehn CE (1940) Bulletin of the Netherland Indies Volcanological Survey. Mining and Geological Department, Bandung, p 89
Stoepke F, Ikari MJ, Hampel A, Meredew K, Watt S, Cassidy M, Urlaub M (2025) Deformation and gravitational instability at Anak Krakatau (Sunda Strait, Indonesia): insights from direct shear experiments and finite-element models. J Geophys Res Solid Earth 130(5):e2024JB030544. https://doi.org/10.1029/2024JB030544
Thorarinsson S (1967) The Surtsey eruption and related scientific work. Polar Rec 13(86):571–578. https://doi.org/10.1017/S0032474000058113
Thornton IWB, Rosengren NJ (1988) Zoological expeditions to the Krakatau Islands, 1984 and 1985: general introduction. Philos Trans R Soc Lond B Biol Sci 322(1211):273–316. https://doi.org/10.1098/rstb.1988.0126
Umbgrove JHF (1928) The first days of the new submarine volcano near Krakatoa. Leidse Geol Meded 2(1):325–328
Unknown (1930) "Geboorte" van Anak Krakatau [Photograph]. Fotocollectie Spaarnestad Onderwerpen, Nationaal Archief (505057_006). http://hdl.handle.net/10648/b04f9403-a56c-bdea-a1a0-26e9d8b357a4
Unknown (1951) De krater het jonge eruptiepunt van de Krakatau-vulkanen. [Photograph]. Collectie Stichting Nationaal Museum van Wereldculturen, Netherlands (TM-10004049). https://hdl.handle.net/20.500.11840/8893
Urlaub M, Belo J, Berndt C, Klein E, Wollschläger J, Völsch A (2023) Reconstructing volcanic eruptions and tsunamis of Krakatau Volcano-Transit, Cruise No. SO299/2, 15.08. 2023–02.09. 2023, Singapore (Singapore)–Port Louis (Mauritius) REE_T BIO-OPS_2023
Van Bemmelen RW (1941) Bulletin of the Netherland Indies Volcanological Survey. Mining and Geological Department, Bandung, No. 91–94
van der Sleen WGN (1929a) De Anak Krakatau. [Photograph]. Collectie Stichting Nationaal Museum van Wereldculturen, Netherlands (TM-10027438). https://hdl.handle.net/20.500.11840/323143
van der Sleen WGN (1929b) Gezicht vanaf zee op de vulkanen Krakatau en Anak Krakatau [Photograph]. Collectie Stichting Nationaal Museum van Wereldculturen, Netherlands (TM-10027436). https://hdl.handle.net/20.500.11840/323115
van Wyk de Vries B, Davies T (2015) Chapter 38—Landslides, debris avalanches, and volcanic gravitational deformation. In H. Sigurdsson (Ed.), The Encyclopedia of Volcanoes (Second Edition) (pp. 665–685). Academic Press. https://doi.org/10.1016/B978-0-12-385938-9.00038-9
Verbeek RDM (Rogier D. M. (with unknown library) (1885) Krakatau. Batavia : Imprimerie de l'état. http://archive.org/details/krakatau00verbgoog
Walter TR, Haghshenas Haghighi M, Schneider FM, Coppola D, Motagh M, Saul J, Babeyko A, Dahm T, Troll VR, Tilmann F, Heimann S, Valade S, Triyono R, Khomarudin R, Kartadinata N, Laiolo M, Massimetti F, Gaebler P (2019) Complex hazard cascade culminating in the Anak Krakatau sector collapse. Nat Commun 10(1):4339. https://doi.org/10.1038/s41467-019-12284-5
Watt SFL (2019) The evolution of volcanic systems following sector collapse. J Volcanol Geotherm Res 384:280–303. https://doi.org/10.1016/j.jvolgeores.2019.05.012
Watt SFL, Karstens J, Micallef A, Berndt C, Urlaub M, Ray M, Desai A, Sammartini M, Klaucke I, Böttner C, Day S, Downes H, Kühn M, Elger J (2019) From catastrophic collapse to multi-phase deposition: flow transformation, seafloor interaction and triggered eruption following a volcanic-island landslide. Earth Planet Sci Lett 517:135–147. https://doi.org/10.1016/j.epsl.2019.04.024
White GS (1947) Anak Krakatau, Sunda Strait October 1947 [Photograph]. X.com (profile @andumkatresnan). https://x.com/andumkatresnan/status/1332984036898193409?s=46
Williams R, Rowley P, Garthwaite MC (2019) Reconstructing the Anak Krakatau flank collapse that caused the December 2018 Indonesian tsunami. Geology 47(10):973–976. https://doi.org/10.1130/G46517.1
Zen MT (1970) Growth and state of Anak Krakatau in September 1968. Bull Volcanol 34(1):205–215. https://doi.org/10.1007/BF02597786
Zen MT, Hadikusumo D (1964) Recent changes in the Anak-Krakatau volcano. Bull Volcanol 27(1):259–268. https://doi.org/10.1007/BF02597525
Zorn EU, Vassileva M, Walter TR, Darmawan H, Röhler L, Amelung F (2023) Interactions of magmatic intrusions with the multiyear flank instability at Anak Krakatau volcano, Indonesia: insights from InSAR and analogue modeling. Geology 51(4):340–344. https://doi.org/10.1130/G50693.1

Authors and Affiliations

Kerys Meredew[1] · Sebastian F. L. Watt[1] · Mike Cassidy[1] · Achmad Fakhrus Shomim[2] · Muhammad Edo Nurshal[3,4] · Mirzam Abdurrachman[4] · Muhammad Hanif[2,5] · Wilfridus F. S. Banggur[2] · Dini Nurfiani[2] · Samantha Engwell[6] · Victoria C. Smith[7] · Chiara M. Petrone[8] · Carl T. E. Stevenson[1] · Devy Kamil Syahbana[9]

✉ Kerys Meredew
kxm574@student.bham.ac.uk

1 School of Geography, Earth and Environmental Sciences, University of Birmingham, Edgbaston, Birmingham, UK

2 Research Center for Geological Disaster, National Research and Innovation Agency (BRIN), Bandung, Indonesia

3 Department of Geosciences, Penn State University, University Park, Pennsylvania, USA

4 Faculty of Earth Sciences and Technology, Bandung Institute of Technology, Bandung, Indonesia

5 Geospatial Imaging and Information Research Group (GI2RG), Faculty of Built Environment and Surveying, Universiti Teknologi Malaysia, Johor Bahru, Malaysia

6 British Geological Survey, The Lyell Centre, Edinburgh, UK

7 Research Laboratory for Archaeology and the History of Art, School of Archaeology, University of Oxford, Oxford, UK

8 Volcano Petrology Group, Natural History Museum, Cromwell Road, London, UK

9 Center for Volcanology and Geological Hazard Mitigation, Geological Agency, Ministry of Energy and Mineral Resources of Indonesia, Bandung, Indonesia